A Probabilistic Deformation-based Seismic Hazard Model for Iran

Alireza Lotfi
IIEES: International Institute of Earthquake Engineering and Seismology
Hamid Zafarani (h.zafarani@iiees.ac.ir)
International Institute of Earthquake Engineering and Seismology https://orcid.org/0000-0002-4431-9692
Alireza Khodaverdian
EPFL: Ecole Polytechnique Federale de Lausanne

Research Article

Keywords: Seismic hazard analysis, Iranian Plateau, Deformation-based model, Earthquake occurrence rate, Earthquake catalog.

Posted Date: February 14th, 2022

DOI: https://doi.org/10.21203/rs.3.rs-1330373/v1

A Probabilistic Deformation-based Seismic Hazard Model for Iran

A. Lotfi[1], H. Zafarani[1*], A. Khodaverdian[2]

[1] International Institute of Earthquake Engineering and Seismology, Tehran, Iran.

[2] Currently at EESD, ENAC, École polytechnique fédérale de Lausanne.

Formerly at Swiss Seismological Service, ETH Zurich, Sonneggstrasse 5, 8092 Zurich, Switzerland.

*Corresponding Author

Declarations

Funding: 'Not applicable'

Conflicts of interest/Competing interests: There is no conflicts of interests

Availability of data and material: 'Not applicable'

Code availability: 'Not applicable'

Abstract

Probabilistic seismic hazard analysis, as the most prevalent approach to evaluate earthquake hazard, is commonly based on earthquake catalogs. Although previous studies show that the recurrence time of large-magnitude (M_w > 7.0) events in Iran is more than ~1000-2000 years, the available instrumentally recorded earthquakes are limited to less than 100 years. With the idea of having another proxy for seismicity rates, we propose a methodology to evaluate activity rates from strain rates in a combination of regional estimates of β and $m_{\max}$. Considering the comprehensive deformation model of the Iranian Plateau, we found that the deformation-based occurrence rates are more than the catalog-based occurrence rates in all seismotectonic provinces in the Iranian Plateau. Except for Central Iran, the ratios of the deformation-based to the catalog-based occurrence rate are between 1.21-3.95. For the first time, a probabilistic deformation-based seismic hazard model for the Iranian plateau is also developed and Peak Ground Acceleration (PGA) values for 10% and 2% POEs in 50 years are estimated. The highest levels of PGA are found in the Azerbaijan and Alborz seismotectonic provinces, where the highest value of strain rates is located. The spatial averages of PGA with 10% POE in 50 years from the deformation-based model are up to 30% higher than the results of a traditional probabilistic seismic hazard for almost all provinces except the Zagros region.

***Keywords**: Seismic hazard analysis, Iranian Plateau, Deformation-based model, Earthquake occurrence rate, Earthquake catalog.*

1. Introduction

Large-magnitude earthquakes have occurred in the Iran Plateau during the long history of this ancient country. Probabilistic Seismic Hazard Analysis (PSHA) is the most prevalent approach to estimate seismic hazard and ground motion parameters. Seismic source model, including source geometry and earthquake occurrence rates, and Ground Motion Prediction Equations (GMPEs) are two main components of PSHA, which play a major role in the Probability of Exceedance (POE) of ground motion parameters at any given site. In the common practice of PSHA, a catalog of historical and instrumental earthquakes is used for the identification of seismogenic sources and quantifying the earthquake occurrence rates (Ghodrati Amiri et al. 2003, Shabani and Mirzaei 2007, Abdollahzadeh et al. 2014a, Khodaverdian et al. 2016b, Khoshnevis et al. 2017). Due to the limited number of large-magnitude instrumentally recorded earthquakes and lack of historical evidence for all faults, rates of large-magnitude earthquakes are usually extrapolated from rates of small-to-moderate ones in the prevalent PSHA (Ward 2007). However, Beauval et al. (2008) showed that, for an earthquake with a 475 years return period, a minimal 12,000 years observation -independent of the seismic activity level is needed to estimate the occurrence rate with a 20% uncertainty. This long required period of observation could be justified by the fact that large-magnitude earthquakes affect the stress state and consequently the size and recurrence time of earthquakes on other adjacent faults, finally causing earthquake rate changes in time (Stein 1999). This fact is also supported by physics-based long-term earthquake simulations in Iran (Khodaverdian et al. 2016a, Khodaverdian et al. 2016c), which showed that long-term seismicity rates should be considered for seismic hazard analyses. Paleoseismological studies (Le Dortz et al. 2009, Le Dortz et al. 2011, Foroutan et al. 2012, Foroutan et al. 2014) also indicate that the recurrence time of large-magnitude earthquakes on a given fault in Iran could be more than 1000-2000 years. In conclusion, while the Iranian earthquake catalog is

69 one of the longest in the world considering the ancient history of the country, it is short
70 relative to the long return period of large-magnitude earthquakes. Occurrence rates of large-
71 magnitude events could be hence underestimated if only incomplete limited available
72 historical evidence, archeological records (Ambraseys and Melville 1982, Berberian 1994,
73 Berberian and Yeats 1999, Berberian and Yeats 2001, Berberian et al. 2014), and short
74 instrumental catalogs are considered.

75 To address the issue of a lack of observed earthquakes, various types of data (e.g.,
76 geological fault slip rates and geodetic data) have been proposed to be used with the
77 accompanying of incomplete earthquake catalogs (Godano and Pingue 2000, Ward 2007,
78 Mazzotti et al. 2011, Danciu et al. 2018). A model that profits from a single type of
79 deformation data or a combination of them can be an alternative way to the estimation of
80 seismic activity rates (Ward 2007). For instance, in the Uniform California Earthquake
81 Rupture Forecast (UCERF3), three deformation models were developed based on geodetic
82 and geologic data and then used in the evaluation of seismic activities (Petersen et al. 2007,
83 Field et al. 2009, Field et al. 2014, Field 2015, Field et al. 2015). As another example,
84 Mazzotti et al. (2011) carried out the probabilistic seismic hazard assessment for continental
85 western Canada based on geodetic data. They used 179 GPS station velocities to obtain
86 regional strain rates.

87 Several geological (Berberian and Yeats 2001, Bachmanov et al. 2004, Allen et al. 2011,
88 Yaminifard et al. 2012) and geodetic investigations (Nilforoushan et al. 2003, Vernant et al.
89 2004b, Masson et al. 2005, Masson et al. 2007) in the Iranian Plateau have been carried out at
90 different scales. GPS measurements were initiated in 1999 and geodetic data is used to
91 quantify the active tectonics of the Iranian Plateau and evaluate the fault slip or strain rates.
92 The first earlier models have built for the whole Iranian Plateau and provided present-day
93 kinematics of the Iranian Plateau using geodetic data (Nilforoushan et al. 2003, Vernant et al.

2004b, Masson et al. 2005, Masson et al. 2007). On the other hand, some local models have been built for smaller seismically active regions (Tatar et al. 2002, Vernant et al. 2004a, Bayer et al. 2006, Hessami et al. 2006, Masson et al. 2006, Walpersdorf et al. 2006, Tavakoli et al. 2008, Djamour et al. 2011, Mousavi et al. 2013, Walpersdorf et al. 2014). A comprehensive summary of these models is presented in section 3. Considering the mentioned studies, there is an opportunity of developing a hazard model from all available deformation data for the Iranian Plateau.

Up to now, several researchers have built PSHA models for the Iranian Plateau with different assumptions (Shabani and Mirzaei 2007, Abdollahzadeh et al. 2014b, Khodaverdian et al. 2016b, Khoshnevis et al. 2017, Zafarani et al. 2017). Khodaverdian et al. (2016b) built a catalog-based seismic hazard model for Iran using the smoothed seismicity approach. Khoshnevis et al. (2017) provided a hazard model for the northern part of Iran based on observed seismicity using the same approach. The Earthquake Model of the Middle East (EMME) is a study, in which both geological data and observed seismicity have been used for seismic hazard assessment of the middle east, including the Iranian Plateau (Danciu et al. 2018, Şeşetyan et al. 2018). The EMME consists of two independent seismogenic source models, area and fault-based source models. Available geological information (i.e., fault trace, and fault slip rates) by that time, together with seismological data (i.e., focal mechanism parameters) have been considered in the development of the fault-based source model. In summary, apart from the EMME, which profits from some deformation data, all available hazard models for the whole or a part of the Iranian Plateau are based on observed seismicity.

In the present study, we are aimed to present the first probabilistic deformation-based hazard model for Iran. In the following section, a brief summary of the tectonic setting of the Iranian Plateau is first presented. Next, we summarize available deformation models for Iran

and select the most comprehensive one, which is used for activity rate estimation and hazard model development. In section 4, a methodology for earthquake occurrence rates estimation from the strain rates is presented, and then estimated rates for the Iranian Plateau are compared with catalog-based seismicity rates. In section 5, a deformation-based seismic hazard model is developed using the estimated earthquake occurrence rates. The characteristics of seismogenic sources and uncertainty considerations are also summarized. Finally, the outputs of our deformation-based seismic hazard model have been presented as hazard maps and hazard curves, and a comparison with other recent seismic hazard models is presented in the last part.

2. Tectonic setting of the Iranian Plateau

The Iranian Plateau is located between the northward moving Arabian Plate and the Eurasian continent (Berberian 1981). The main tectonic regime has resulted from a convergence between the Eurasian and Arabian plates, which occurs at a rate of ~31 mm/year at the longitude of 52°E (Vernant et al. 2004b). Approximately rigid aseismic blocks (e.g., Central Iranian Block (CIB), South Caspian Block (SCB), and Lut Desert Block (LDB)) are surrounded by deforming belts (e.g., Zagros, Alborz, Kopeh Dagh, and Talesh) (Nowroozi 1976, Jackson et al. 1995, Walker and Jackson 2004, Khodaverdian et al. 2015).

Several studies categorized the Iranian Plateau into various seismotectonic provinces according to the tectonic, geologic information, and the quantitative observations of seismic events (StScklin 1968, Takin 1972, Berberian 1976a, Berberian 1976b, Ansari et al. 2009). The seismotectonic map, proposed by Mirzaei et al. (1998), is one of the commonly used categorizations, in which the Iranian Plateau is divided into five major tectonic zones, including Azerbaijan-Alborz, Kopeh Dagh, Zagros, Central-East Iran, and Makran. We

considered the map of the seismotectonic provinces presented by Mirzaei et al. (1998) as a base and separated Azerbaijan-Alborz and Central-East Iran into two parts so that seven seismotectonic provinces (i.e., Azerbaijan, Alborz, Kopeh Dagh, Zagros, Central Iran, Eastern Iran, and Makran) are finally considered for the Iranian Plateau (Figure 1). Also shown in Figure 1 is a homogenized earthquake catalog compiled by Shahvar et al. (2013) and updated by Khodaverdian et al. (2016b). All earthquakes in the Iranian plateau are shallow crustal events, with focal depths less than 40 km, except events in the Makran subduction zone, southeast Iran, where deeper earthquakes (in-slab or interface earthquakes) could occur (Mirzaei et al. (1998). The Makran region is excluded from the current study as shallow crustal deformation data could not be directly informative for seismicity estimation. The major faults and seismic characteristics of provinces are summarized in the following.

Alborz seismotectonic province is one of the most active regions in the north of the Iranian Plateau. The Alborz mountain belt is 600 km long and stretches from the Talesh mountains in the west to the Kopeh Dagh mountains in the east along the southern side of the Caspian Sea. Between Central Iran and the SCB, there is oblique convergence, which is observed in the form of the left slip along the Astaneh, Firoozkouh, Mosha, and Taleghan faults and perpendicular movement along the Caspian and Alborz faults (Ritz et al. 2003, Bachmanov et al. 2004, Nazari 2006, Nazari et al. 2009). The Khazar and North Alborz faults (Bachmanov et al. 2004) are thrust faults located in the north part of the province and some major active faults (e.g., Pishva, Eshtehard, and Ipak faults) are delineated in the south. The North Tehran fault with a 110 km length, is the most hazardous fault near the capital city of Tehran (Ritz et al. 2012). Several historical earthquakes in 743, 958, 1177, 1665, and 1830 are reported for the area close to the city of Tehran (Ambraseys and Melville 1982, Berberian 1994).

Zagros seismotectonic province is the most active seismic region in the Iranian Plateau, which absorbed a large amount of the total deformation from the Arabian-Eurasia convergence. Zagros fold-and-thrust belt with 250–400 km width is extended from eastern Turkey to the Strait of Hormoz. The northwest part of Zagros is affected by orogen-parallel thrust faults, and the large Main Recent Fault (MRF), showing partitioning of the oblique motion to the north (Berberian 1995). The right-lateral strike-slip faulting along the MRF is approved by tectonic geomorphology and focal mechanism solutions of earthquakes (Berberian 1995, Berberian and Yeats 2001, Talebian and Jackson 2004, Yamini-Fard et al. 2006). The southeast part of Zagros is characterized by lots of shallow thrust faults and the NW-SE strike of the Zagros fold range turns to almost W-E in this part, east of 52°E, and the belt becomes perpendicular to the Arabia-Eurasia shortening direction.

Azerbaijan seismotectonic province at the northwest of Iran is mostly affected by the North Tabriz fault system with a dominant right-lateral faulting mechanism and NE-SW trend (Jackson and McKenzie 1984, Berberian and Yeats 1999, Karakhanian et al. 2004). Tectonics of the Turkey-Iran-Caucasus region are investigated in several studies (e.g., (Copley and Jackson 2006)) that revealed this region is characterized by partitioning of oblique plate convergence. Earthquakes focal mechanism solutions (Jackson 1992) show thrust faulting in the eastern part of the Greater Caucasus, and the right lateral motion accommodated in the Turkish-Iranian Plateau on strike-slip fault systems (e.g., Chalderan and North Tabriz faults). From 1721 to 1786, during 65 years, the North Tabriz fault has ruptured three times, which includes the M_s 7.7, 1721, the M_s 7.7, 1780, and the M_s 6.3, 1786 earthquakes (Ambraseys and Melville 1982, Berberian 1994). More recently, extensive damages and human losses are caused by the M_w 6.4 and 6.3, 2012 Ahar-Varzaghan double earthquakes.

The Kopeh Dagh province, forming the boundary between the Iranian Plateau and Eurasian plate. The Kopeh Dagh range is confined by the NW-SE trending Main Kopeh

192 Dagh Fault (MKDF) in the northwest and thrust faults in the southeast. The M_w 7.3, 1948
193 earthquake has been ascribed to the MKDF. In the central part of the Kopeh Dagh range, an
194 array of right-lateral strike-slip faults with NNW-trending (i.e., the Baghan-Quchan fault
195 system) obliquely crosses the range and allows Central Iran to move northward with respect
196 to the stable part of Eurasia (Shabanian et al. 2009). There are also some major faults (i.e.,
197 Neyshabur and the Binalud reverse faults), which were responsible for some large historical
198 earthquakes with M_w > 7, that struck near the Neyshabur city between 1209 and 1405
199 (Berberian and Yeats 1999).

200 The central and eastern seismotectonic provinces of Iran encompass aseismic rigid blocks
201 (e.g., CIB), which have been surrounded by seismically active belts (e.g., Alborz and Zagros)
202 (Nowroozi 1976, Jackson et al. 1995, Walker and Jackson 2004). LDB is also surrounding by
203 some fault systems (e.g., Doruneh and Dasht-e-Bayaz faults). These faults are seismically
204 active and responsible for the major destructive earthquakes in the region (e.g., the M_w 7,
205 1968, the M_w 7.3, 1979, and the M_s 7.3, 1978 earthquakes) (Berberian and Yeats 1999,
206 Aghanabati 2004, Walker et al. 2004). Infrequent and large-magnitude earthquakes with
207 recurrence intervals of more than several hundred years are characteristics of Central–Eastern
208 Iran (Berberian and Yeats 1999, Berberian 2014). Although the region experienced
209 infrequent earthquakes during the approximately 2750 years of observation time, according to
210 paleoseismological studies (Le Dortz et al. 2009, Walker et al. 2010, Le Dortz et al. 2011,
211 Foroutan et al. 2012, Foroutan et al. 2014), several large-magnitude earthquakes occurred in
212 the region during the Late Pleistocene and Holocene. These studies have shown that faults
213 without historical seismic evidence in Central–Eastern Iran are responsible for large-
214 magnitude (M_w~7) earthquakes during the Holocene and the contribution of recently silent
215 faults to seismic hazard assessment must be considered.

216

3. Comprehensive deformation and strain rate model for Iran

Several deformation models have been developed for the Iranian plateau based on geological and geodetic information and these models could be classified into two categories. The first category is global models that provide a large-scale perspective of the Iranian Plateau's present-day kinematics, plate motions in the Middle East, and gross deformation across various active belts (Nilforoushan et al. 2003, Vernant et al. 2004b, Masson et al. 2005, Masson et al. 2007). The second category is local models that have been built for smaller seismically active regions in the Plateau using block modeling techniques to provide detailed active deformation of different fault systems in Iran (Tavakoli et al. 2008, Djamour et al. 2011, Mousavi et al. 2013, Walpersdorf et al. 2014). However, some drawbacks of the block modeling technique are: (1) some blocks are poorly represented by the rigid block model due to the existence of small faults in the region, (2) an array of active strike-slip faults are simplified and modeled by only one boundary fault, and (3) the GPS stations are still too sparse, particularly around the secondary faults, so few secondary fault slip rates are derived, while lots of minor faults in the Iranian plateau need to be considered in a proper strain modeling (Khodaverdian et al. 2015).

Khodaverdian et al. (2015) presented the first comprehensive deformation model, in which the long-term crustal flow of the Iranian Plateau is computed by using various data sets, including fault traces, geologic fault offset rates, GPS velocities, principal stress directions, and velocity boundary conditions. As input, the long-term geological offset rates for 33 of 171 fault traces were collected based on the available data on relative displacement of geologic features. Also, geodetic velocities of 239 GPS benchmarks, together with data from the world stress map were considered. The main outcome of the model is strain rates and fault slip rates, which are the most up-to-date evaluation at the regional scale. The

241 estimates of fault slip rates have been also validated with slip rates resulted from analyzing
242 geodetic velocities, or geological/paleoseismological studies, which have not been used in the
243 model calibration.

244 When solely GPS data are used in developing a deformation model, an important step is
245 required to limit the perturbing impacts of transient and surficial processes in the earth. Bird
246 and Carafa (2016) and Carafa and Bird (2016) demonstrate that these effects of transient and
247 surficial signals are significantly minimized when the augmented covariance matrix is
248 utilized in the objective function for a deformation model, primarily driven by GPS data.
249 They also showed that the successful application of their method should be investigated by
250 comparing the GPS-based deformation model with a comprehensive model, in which several
251 datasets (e.g., plate-tectonic velocity boundary conditions, geological fault traces and their
252 slip rates, and the most compressive horizontal principal stress directions) are used. As the
253 Khodaverdian et al. (2015)'s model is developed based on several different long-term input
254 datasets, and their estimated rates are consistent with independent long-term geological rates,
255 their output (i.e., strain rates) provides a picture of long-term deformation in the study area
256 and is the viable candidate for further calculation of moment and seismic activity rates (see
257 section 4.2 for more details).

258

259 ## 4. Seismic activity rate from deformation model

260 In the following section, we first present a methodology to evaluate the earthquake
261 occurrence rate from the strain rate. The total moment rates for the Iranian Plateau are
262 evaluated from two available strain rate models by the implementation of the proposed
263 method. Next, the estimated earthquake occurrence rates are compared with catalog-based

264 seismicity rates. We also carried out a sensitivity analysis to study the effect of seismogenic
265 layer thickness on the estimated earthquake occurrence rates from strain rates.

266

267 **4.1. Methodology**

268 The first step to estimate earthquake occurrence rates is to evaluate seismic moment rate
269 $(\dot{M}_0)$ from strain rates using the following equation (Savage and Simpson 1997):

$$\dot{M}_0 = 2\mu A h \mathrm{Max}(|\dot{\varepsilon}_1|, |\dot{\varepsilon}_2|, |\dot{\varepsilon}_1 + \dot{\varepsilon}_2|) \quad (1)$$

270

271 where μ is the average rigidity of the crust, A is the area of the source zone, and h is the
272 seismogenic thickness of the crust. $\dot{\varepsilon}_1$ and $\dot{\varepsilon}_2$ are the principal components of the strain rate
273 tensor. As presented in equation (2), by assuming double truncated Gutenberg-Richter
274 relation, the occurrence rate of earthquakes with equal to or larger than minimum magnitude,
275 $\lambda(m_0)$, can be given by the following equation (e.g., (Anderson and Luco 1983)):

$$\lambda(m_0) = \frac{\dot{M}_0}{\int_{m_0}^{m_{\max}} f_m(m) M_0(m) dm} \quad (2)$$

276

277 where $\dot{M}_0$ is the seismic moment rate, m_0 and $m_{\max}$ are the minimum and maximum
278 magnitude, respectively. $M_0(m)$ is the seismic moment, which is released by an earthquake
279 with magnitude m, and can be evaluated by the well-known relation of Hanks and Kanamori
280 (1979) as following:

$$M_0(m) = 10^{cm+d} \quad (3)$$

281

where c equals 1.5 and d takes the values 9.05 or 16 to estimate the seismic moment in units of N.m or dyne.cm, respectively. Tab,represents frequency-magnitude probability density function for double truncated Gutenberg-Richter distribution (G-R distribution):

$$f_m(m) = \frac{\beta \exp[-\beta(m - m_0)]}{1 - \exp[-\beta(m_{\max} - m_0)]} \quad for \quad m_0 \le m \le m_{\max} \tag{4}$$

where $\beta = b \ln 10$ is the slope of the G-R distribution.

Considering equations (1-4), $\dot{M}_0$, which is obtained from the strain rates, could be converted to $\lambda(m_0)$ given that β, m_0, and $m_{\max}$ are available for the study area. Spatial variation of β and $m_{\max}$ are not as high as seismic activity rate; β and $m_{\max}$ are mostly presented as regional parameters and can be estimated from the catalog of observed earthquakes for a given region (Kijko et al. 2016). In other words, fault-specific or source-specific β -values are rarely used in hazard studies due to the lack of sufficient data. It is very common to construct super zones and evaluate a regional β -value and assign it to all inner zones (see e.g., (Field et al. 2014, Field et al. 2015, Danciu et al. 2018, Şeşetyan et al. 2018)). The lower bound or minimum magnitude (m_0) is chosen on the basis that events with lower magnitude are mostly ignored by engineers. A review of practice reveals that values of m_0 generally lie in a range of 4-5. In the present study, the minimum magnitude is set as 4.0. In summary, the regional estimate of β and $m_{\max}$ from the statistics of observed seismicity can be hence a suitable value to be considered as an input for the proposed methodology and the deformation-based seismicity rate, $\lambda(m_0)$, can be eventually evaluated by using all the aforementioned equations.

303 **4.2. Total moment rates for the Iranian Plateau**

304 Deformation-Based Strain Rate Model (DBSRM) presented by Khodaverdian et al. (2015) is
305 the most up-to-date and comprehensive model for the Iranian Plateau. The strain rates from
306 that model are converted into the deformation-based total moment rates ($\dot{M}_0^{D,total}$) (see Figure
307 2a) by using equation (1) and assuming $\mu = 27.7$ GPa, as suggested by Bird and Kagan
308 (2004) for a continental convergent boundary. The highest values of $\dot{M}_0^{D,total}$ are concentrated
309 along faults, located in major seismically active belts (e.g., the Zagros, Alborz, and Kopeh
310 Dagh mountains). Moment rates in central and eastern Iran (e.g., the CIB and LDB) are
311 generally low while high moment rates can also be seen along the faults surrounding the
312 LDB. Although DBSRM covers the whole Iranian Plateau, the current study focuses on the
313 crustal seismic sources and does not include the Makran subduction region, located in
314 southeastern Iran. Moment rate estimates for that region will be presented in future papers by
315 combining the results of the ongoing research projects aiming to capture a better picture of
316 the seismogenic layer in that region.

317 Another available deformation model covering the whole Iranian Plateau is the Global
318 Strain Rate Model (GSRM), which is the purely geodetic-based model by (Kreemer et al.
319 2014). Figure 2b shows the spatial distribution of the total moment rates derived from GSRM
320 using equation (1) for the whole Iranian Plateau. Comparison of Figure 2a with Figure 2b
321 shows that both models evaluate high moment rates in the Alborz, Azerbaijan, Kopeh Dagh,
322 and Zagros seismotectonic provinces. For instance, total moment rate values, derived from
323 DBSRM and GSRM, for the area close to the city of Tehran are 2.31E+13 (Nm/yr/km^2) and
324 1.69E+13 (Nm/yr/km^2), respectively. As another example, the rates derived from DBSRM
325 and GSRM, for the area close to the city of Tabriz, located in Azerbaijan, are 13.17E+13
326 (Nm/yr/km^2) and 4.13E+13 (Nm/yr/km^2), respectively. Comparison of Figure 2a with Figure

2b also shows that DBSRM generally gives higher rates for Central Iran and Eastern Iran since the geological slip rates for active faults in Central Iran (e.g., the Dehshir, Anar, Nayband, Nehbandan, and Nosratabad faults) are also considered in DBSRM.

GSRM and DBSRM are different in terms of scale and inputs. While GSRM is developed based on geodetic data on a global scale, DBSRM is built at a local scale and covers only the Iranian Plateau, which provided the opportunity of profiting from various deformation datasets (e.g., geological and geodetic data and principal stress directions). Considering the finer details used in DBSRM, moment rates derived from DBSRM are selected to be used in the next step of earthquake occurrence rates evaluation.

4.3. Deformation-based activity rate and its comparison with observed seismicity

The total moment rate, which is estimated based on the strain rate, encompasses both seismic and aseismic deformation. With the goal of seismic hazard assessment, it is necessary to estimate the seismic fraction of the deformation-based moment rate ($\dot{M}_0^D$) from the total moment rate ($\dot{M}_0^{D,total}$). In other words, the portion of aseismic deformation should be removed from the total moment rate before the calculation of earthquake occurrence rates. Khodaverdian et al. (2015) used Ward's statistical analyses, (Ward 1998) by which a relationship between the ratio of the observed seismic moment to the total seismic moment, earthquake catalog length, and strain rate are presented. Considering 100-years and 200-years seismic catalogs for the Iranian Plateau, two estimates of seismic deformation fraction (η) for the Azerbaijan, Alborz, Kopeh Dagh, and Zagros seismotectonic provinces are evaluated. It is shown that the Zagros province accommodates considerable aseismic deformation while Alborz and Azerbaijan release a major part of accumulated strain in seismic events. As η is not provided for Central Iran and Eastern Iran by Khodaverdian et al. (2015), we here

351 estimated that parameter for those provinces based on the same approach, as described. The
352 final results showed almost all the deformations in these two seismotectonic provinces are
353 released in seismic events; η is equal to 0.95 for Central Iran and Eastern Iran. The values of
354 η for all seismotectonic provinces are summarized in Table 1 and applied to the total moment
355 rates in the process of deformation-based earthquake occurrence estimation.

356 As described in section 4.1, β and $m_{\max}$ are required seismicity parameters in the
357 evaluation of the deformation-based earthquakes occurrence rates. These parameters are
358 calculated by the maximum likelihood procedure of Kijko et al. (2016) from the observed
359 seismicity after removing aftershocks and foreshocks. The homogenized earthquake catalog,
360 compiled by Shahvar et al. (2013) and updated by Khodaverdian et al. (2016b), is used. M_w is
361 chosen as a reference magnitude, and the entire earthquake catalog is declustered using
362 Gardner and Knopoff (1974) approach. As the catalog consists of historical and instrumental
363 earthquakes of the Iranian plateau, using Stepp (1972) completeness criteria, the historical
364 and instrumental parts are precisely separated. The instrumental section is also examined to
365 find the various completeness intervals by using the maximum curvature method (Wiemer
366 and Wyss 2000). Generally, the seismic earthquake catalog available for the Iranian plateau
367 can be roughly divided into three periods. The first period contains evidence of historical
368 earthquakes up to the beginning of the twentieth century. The second period (1900 to ~1970)
369 is a transition between the period of historical data and the modern instrumental period,
370 although the installation of the first seismographic instruments in Iran was performed during
371 the earlier decades of the past century. The third period starts in 1970, since which the
372 obtained seismic data is purely instrumentally recorded due to the adequate density of the
373 regional network. Having historical and instrumental parts of the earthquake catalog, together
374 with the completeness magnitude for each time interval from the maximum curvature
375 method, we estimated long-term catalog-based occurrence rates of earthquakes with

magnitudes equal to or larger than M_w 4.0 (λ_4^C). Those, together with β, and $m_{\max}$ and long-term catalog-based seismic moment rates ($\dot{M}_0^C$)for all seismotectonic provinces in the Iranian Plateau are summarized in Table 2.

Considering the regional estimates of β, $m_{\max}$, η_{ave} and assuming the minimum magnitude of 4.0 ($m_0 = 4.0$), we calculated deformation-based occurrence rates of earthquakes with magnitude equal to or larger than M_w 4.0 (λ_4^D) for all provinces using the proposed method in section 4.1. As shown in Table 2, the deformation-based earthquake occurrence rates are higher than the catalog-based occurrence rates; $\lambda_4^D / \lambda_4^C$ varies from 1.21 to 8.88. Except for Central Iran, the average of $\lambda_4^D / \lambda_4^C$ is 2.9 for other provinces. The lowest amount of $\lambda_4^D / \lambda_4^C$ is observed for the Zagros province. In this province, earthquakes with relatively short recurrence times occur (Talebian and Jackson 2004, Kalaneh and Agh-Atabai 2016) and, as a result, less discrepancy between deformation-based and catalog-based earthquakes rates is expected. The maximum amount of $\lambda_4^D / \lambda_4^C$ corresponds to Central Iran, where large-magnitude earthquakes occur with long recurrence times (Berberian and Yeats 2001) and in earthquakes have been recorded. For the Central Iran and Eastern Iran provinces, the values of $\lambda_4^D / \lambda_4^C$ are estimated at 8.88 and 3.95, respectively. The values of $\lambda_4^D / \lambda_4^C$ for the Azerbaijan, Alborz, and Kopeh Dagh provinces are varying between the minimum and maximum values, which is consistent with the fact that the recurrence times of the large-magnitude earthquakes in these provinces are less frequent than Zagros and more frequent than Central Iran and Eastern Iran. To have a full picture of the comparison between catalog-based and deformation-based earthquake occurrence rates, Frequency-Magnitude Distribution (FMD) for all seismotectonic provinces is depicted in Figure 3.

A wide range of deformation-based to catalog-based moment rate ratios have been reported in different investigations. For example, Mazzotti et al. (2011) use regional strain rates obtained from GPS velocities to test an alternate PSHA method in continental western Canada. They reported that the range of 1.2 to 3×10^4 for the mean ratio of the deformation-based moment to catalog-based seismic moment. They referred this considerable discrepancy to an under-sampling of long-term moment rates and poor earthquake catalogs in some zones. Bungum et al. (2017) also compared seismic moments derived from strain rates with those derived from earthquake catalogs for six segments along the Himalayan arc. The ratio of strain-based moment rate to catalog-based moment rate varies from 1.05 to 56.62. The segment with the highest discrepancy is characterized by low active seismicity in the Himalayan arc (Rajendran et al. 2013). Srivastava et al. (2015) also provide a detailed review of the seismic gaps and noted that different areas in Himalaya may not be equally seismogenic. Similarly, Central Iran is characterized by approximately rigid blocks (Nowroozi 1976, Jackson et al. 1995, Walker and Jackson 2004). Infrequent and large-magnitude earthquakes with recurrence intervals of more than several hundred years are characteristics of Central–Eastern Iran (Berberian and Yeats 1999, Berberian 2014), which could be a justification for the high value of $\lambda_4^D / \lambda_4^C$ (i.e., 8.88).

According to paleoseismological studies (Le Dortz et al. 2009, Walker et al. 2010, Le Dortz et al. 2011, Foroutan et al. 2012, Foroutan et al. 2014), several large-magnitude earthquakes occurred in the region during the Late Pleistocene and Holocene while some of them have not been recorded because of lack of historical evidence. These studies have also shown that faults in Central–Eastern Iran are responsible for infrequent large-magnitude (M_w~*7*) earthquakes. Therefore, M_w~7 could be a representative of large-magnitude earthquakes in these provinces (Berberian et al. 2014, Mousavi-Bafrouei et al. 2015) and we investigate the number of Mw 7.0 earthquakes in 100 years based on catalog-based

occurrence rate (N_7^C) and its difference to the corresponding deformation-based estimates (N_7^{D-C}). As shown in Table 2 in the manuscript, for Central Iran province, the amount of N_7^{D-C} is 1.47. Given that Central–Eastern Iran is characterized by those large-magnitude earthquakes, the high value of $\lambda_4^D / \lambda_4^C$ for that region can be justified by a few missed M_w 7.0 earthquakes in the historical evidence.

4.4. Sensitivity analysis for seismogenic layer thickness

The seismic moment rate is dependent on the seismogenic layer thickness (h in equation (1)). Using sensitivity analysis of seismogenic layer thickness, we investigated the effect of h variations on the $\lambda_{m_0}^D$ and G-R distribution. In Table 3, $\lambda_{m_0,h}^D$, occurrence rates of the M_w 4.0+ earthquakes for each seismotectonic province for given seismogenic thicknesses of 10, 15, and 20 km are presented; these three values are based on the depths of observed seismicity (Engdahl et al. 2006). As an example, for the Zagros province, the deformation-based G-R distributions with different $\lambda_{m_0,h}^D$ for 10, 15 km, and 20 km seismogenic layer thicknesses are shown in Figure 4. Also, the catalog-based G-R distribution and its corresponding uncertainty are shown in Figure 4. Comparing these curves shows that the uncertainty of h is comparable with the uncertainties of β and λ_4^C, which are derived from observed seismicity. Therefore, variation of seismogenic layer thickness has a considerable effect on the estimated activity rate values and consequently should be considered in the seismic hazard analyses.

5. Seismic hazard assessment

Deformation-Based Hazard Model (DBHM) and its details are presented in the following section. We defined the geometry and characteristics of seismogenic sources using two categories of data (section 5.1) and then activity rates for these sources are assigned from long-term estimates we have from the deformation model. In section 5.2, the GMPEs used in the model are presented. Logic tree method for capturing the uncertainties of seismogenic layer thickness, maximum magnitude, β -values, seismic deformation fractions, and GMPEs are considered and described in section 5.3.

5.1. Seismic area sources

From the selected comprehensive deformation model for the Iranian Plateau, the strain rate field is available for a grid of $0.2^{o} \times 0.2^{o}$ cells. Square area sources, with the same size and spacing, are considered to cover the whole Iranian Plateau (Figure 5). The estimate of β, and m_{max} for the Iranian Plateau on a grid of $1^{o} \times 1^{o}$ degrees is available from Khodaverdian et al. (2016b). Although the regional estimate of β, and m_{max} for each seismotectonic province is provided in section 4.3, we used the estimates on a grid of $1^{o} \times 1^{o}$ to better capture the spatial variation of these parameters and allocated them to square area sources based on the nearest neighbor rule. Using these values and assuming the minimum magnitude of 4.0 ($m_0 = 4.0$), we then calculated the deformation-based earthquake occurrence rate (λ_4^D) for each square area source, according to the procedure described in section 4.1. It is worth mentioning that uncertainties of the regional estimate of β and m_{max}, provided by Khodaverdian et al. (2016b), are also taken into the account (refer to section 5.3 for more details).

466 The characteristics of seismic sources are usually based on tectonic, geological, and
467 seismological evidence. One of the important parameters of seismic source modeling is the
468 depth of the seismogenic layer. Since the tectonic setting throughout a province is similar
469 (Hong et al. 1996), we assign the identical hypocentral depths to area sources located in the
470 same provinces. We used the map of seismotectonic provinces of the Iranian Plateau
471 presented by Mirzaei et al. (1998) (Figure 1) and hypocentral depth for the different
472 provinces is evaluated from available studies. For example, Mooney et al. (1998) suggested
473 that seismicity in eastern Iran is restricted to the upper continental crust with a seismogenic
474 thickness of ~15 km (Maggi et al. 2000), also moderate-to-large magnitude earthquakes
475 occurred with a median depth of 12±5 km (Zare et al. 2014). More recently, Engdahl et al.
476 (2006) have reported precise earthquake depth distribution for the seismotectonic provinces
477 of the Iranian Plateau. For the Alborz, the range of earthquake depths is 5-30 km, while more
478 earthquakes occur at a depth of 5-15 km and these values for Eastern Iran are 0-20 km and 5-
479 15 km, respectively (Engdahl et al. 2006). Zare et al. (2014) presented a depth of 11 km for
480 most of the earthquakes that occurred in the Alborz and Azerbaijan. A depth of 15 km for
481 most of the earthquakes in the Kopeh Dagh and Central Iran and a depth of 13 km for the
482 earthquakes in the Zagros are reported. According to the mentioned studies, we considered
483 the hypocentral depth of 10 km, 15 km, and 20 km with the probabilities of 0.333, 0.334, and
484 0.333, respectively, for the Zagros province. For all other seismotectonic provinces, we
485 considered the hypocentral depth of 7.5 km, 12.5 km, 17.5 km, 22.5 km, 27.5 km with the
486 probabilities of 0.375, 0.375, 0.125, 0.0625, and 0.0625, respectively.

487 The surrounding zones around the mapped active faults are one of the major seismic
488 sources as the concentration of seismic moment within narrow zones along the faults is
489 shown in Figure 2a. The characteristics of faults should be considered in seismic source
490 modeling for these zones. Hence, near-fault zones are defined as a band of 15 km on each

side along the active faults. As shown in Figure 5, a total of 15, 3, 8, 8, 4, and 17 near-fault zones in the Alborz, Zagros, Azerbaijan, Kopeh Dagh, Central Iran, and Eastern Iran provinces are considered, respectively. Active faults maps of Iran are provided in some studies (e.g., Hessami et al. (2013) and Danciu et al. (2018)) (see Figure 5) and the fault plane characteristics are reported in different studies (e.g., Khodaverdian et al. (2016a) for Azerbaijan, Khodaverdian et al. (2016c) for Eastern Iran, and Bachmanov et al. (2004) for the Zagros and Central Iran). Those studies and the references therein have been used to define the predominant faulting plane characteristics (i.e., strike, dip, and rake) of near-fault zones. If a given square area $0.2^{o} \times 0.2^{o}$ source is located within a near-fault zone, the characteristics of the corresponding near-fault zone are assigned to the area source. For area sources located outside of near-fault zones, the average of the faulting characteristics of all faults located in the corresponding seismotectonic province is used.

5.2. Ground Motion Prediction Equations

GMPE is a key element in PSHA as it estimates the intensity level at a particular site given a specified earthquake. Cotton et al. (2006) point out some criteria that could be used for GMPE selection from a list of candidate models. They suggested that the GMPE model should have adequate documents and obtained from a relevant tectonic regime and should be published in an international peer-reviewed journal. The model outcome range should be proper for engineering applications and has a suitable functional form. Bommer et al. (2010) modified the Cotton et al. (2006) criteria and provided a more complete set of criteria. For example, they presented that the model must use appropriate definitions for parameters (e.g., magnitude and distance) and has the consideration of site effect with the average shear-wave velocity for the upper 30-m depth, denoted as V_{s30}.

Based on previous experiences published in several peer-reviewed papers (e.g., Mousavi et al. (2012), Zafarani and Mousavi (2014), and Zafarani and Farhadi (2017)) and others (e.g., Shoja–Taheri et al. (2010)) which examine the local, NGA or regional GMPEs performance for Iran, a combination of regional, NGA and local GMPEs is a rational choice for hazard analysis in Iran, from the viewpoint of capturing epistemic uncertainty.

Based on data-driven statistical evaluations, it can be concluded that local models usually provide a good explanation of recorded strong motion data in Iran (e.g., Mousavi et al. (2012), Zafarani and Mousavi (2014), and Zafarani and Farhadi (2017)). However, due to the scarcity of near-field records, their performance in the prediction of near-field motions of large earthquakes is a matter of debate. The database of regional and NGA GMPEs are richer in the near-field region, thanks to gathering data from diverse shallow crustal regions. For example, the NGA-WEST2 contains data from large earthquakes that occurred in Alaska, Mexico, Greece, Turkey, Iran, Taiwan, China, New Zealand, Japan, and Italy.

Finally, we select five local, regional, and global GMPEs for seismic hazard assessment. The first one is Zafarani et al. (2018), a local GMPE, which is developed based on a comprehensive, compiled, and good-quality strong-motion database of the Iranian earthquakes. The second one is Kale et al. (2015), a regional GMPE, which is developed for Turkey and Iran to investigate the possible regional effects on ground-motion amplitudes in active shallow crust earthquakes. This GMPE is based on a subset of the compiled strong-motion database of the Earthquake Model of the Middle East (EMME) project (Danciu et al. 2018, Şeşetyan et al. 2018). The third GMPE is Zhao et al. (2006), which is one of the global GMPEs that was presented based on a large number of strong ground-motion records in Japan. Abrahamson et al. (2014) and Idriss (2014) are global GMPEs that are developed in the NGA-West2 project (Bozorgnia et al. 2014) for shallow crustal earthquakes in active tectonic regions.

Finally, it should be noted that all available GMPEs in Iran are developed based on the simple as the recorded geometric mean of two horizontal components. However, it has been shown by Boore (2010) that as recorded geometric mean of two horizontal components is very similar to the median spectral accelerations over all orientations (RotD50), which NGA-West2 models predict (see Figure 4 in (Boore 2010)). As shown in Figure 6, recorded observed ground motion for the Finn, 2021 dual earthquakes (see Figure 5, where their epicenter are shown) are compared to five selected GMPEs. General compatibility between the geometric mean of the east and north components of Finn dual earthquakes and selected GMPEs for M6.2 with reverse focal mechanism and Vs30=500 m/s is observed.

5.3. Uncertainties consideration

For taking into account possible epistemic uncertainties, the logic tree approach is used. A logic tree consisting of five branching levels (seismogenic layer thicknesses, seismicity parameters (β and $m_{\max}$), seismic deformation fractions, and GMPEs) is proposed (Figure 7). The branch weights in a logic tree framework represent the degree-of-certainty or degree-of-belief of experts in alternative models and parameter values. According to Bommer (2012), the population of logic trees with models that represent both the best estimates on the basis of what is known and alternative models that represent what could occur in light of our lack of knowledge, requires expertise and experience in both the relevant earth science disciplines and in the characterization of uncertainty.

The first branching level shows the uncertainties of the seismogenic layer thicknesses. As shown in section 4.4, variation of seismogenic layer thickness has a considerable effect on the activity rate values and should be considered in the seismic hazard analysis. We considered $h_{\min} = 10$ km, $h_{ave} = 15$ km, and $h_{\max} = 20$ km with the weights of 0.25, 0.5, and 0.25,

564 respectively. The second branching level belongs to the uncertainties of the maximum
565 magnitude. $m_{\max,ave}-\sigma_{m_{\max}}$, $m_{\max,ave}$, and $m_{\max,ave}+\sigma_{m_{\max}}$ with the weights of 0.25, 0.5, and
566 0.25, respectively are considered. The third branching level demonstrates the uncertainties of
567 regional estimates of β. In this branch $\beta_{ave}-\sigma_{\beta}$, β_{ave}, and $\beta_{ave}+\sigma_{\beta}$ with the weights of
568 0.25, 0.5, and 0.25, respectively are considered. The fourth branching level shows the
569 uncertainties of η , which are derived considering 100-years and 200-years seismic catalogs
570 length. η_{100}, η_{ave}, and η_{200} with the weights of 0.25, 0.5, and 0.25 are considered,
571 respectively. The fifth branching level belongs to the uncertainties of the GMPEs. We
572 considered the same weight for all GMPEs that are used here. Here, we attempt to assign
573 numbers to our degrees of belief, which are by nature personal and indefinable, and for which
574 there are neither tests nor measurements. However, in addition to the "expert opinion"
575 approach, we also consider a statistically-based scheme to assign the logic tree weights of
576 GMPEs (Mousavi et al. 2012, Zafarani and Mousavi 2014, Zafarani and Farhadi 2017).

577

578 ## 6. Results

579 The seismic hazard computation is performed with the OpenQuake hazard engine (Pagani et
580 al. 2014), which is an open-source package developed by the GSRM for seismic hazard and
581 risk analyses. We estimate PGA at 10% and 2% POEs in 50 years, which correspond to 475
582 and 2475 years return periods, respectively. Hazard assessment results are presented on
583 bedrock with the V_{s30} of 760 m/s (V_{s30} represents the average velocity of shear waves in the
584 top 30 m of soil). It is a common practice to truncate the lognormal distribution of ground-
585 motion residuals at 2 or 3 times of the standard deviation (Bommer and Abrahamson 2006).
586 Truncating above this level, for the return periods generally used in engineering design, has
587 little effect on the hazard curves; therefore, a truncation value of 3 times of the standard

588 deviation is applied. The outcome is presented as hazard maps and hazard curves and
589 compared with the results of the other probabilistic seismic hazard analyses for the Iranian
590 Plateau.

591

592 **6.1. Hazard maps**

593 Hazard maps of the mean PGA value for 10% and 2% POEs in 50 years are presented in
594 Figures 8 (a) and 8 (b), respectively. The spatial average values of the PGA for the
595 Azerbaijan, Alborz, Kopeh Dagh, Central Iran, Eastern Iran, and Zagros seismotectonic
596 provinces are 0.44 g, 0.38 g, 0.33 g, 0.28 g, 0.29 g, and 0.23 g for 10% POE, respectively.
597 Also, the standard deviations of the PGA values are 0.1 g, 0.09 g, 0.07 g, 0.09 g, 0.08 g, and
598 0.05 g for 10% POE, respectively. According to hazard maps derived from DBHM, the
599 highest PGA are observed in the Azerbaijan and Alborz provinces, where the highest values
600 of strain rates are also located. Also, in the Kopeh Dagh province, high PGA values have
601 been seen in a strip, which is extended from the east of the Alborz to Mashhad city. The strip,
602 covers Robate-Qarabil (RBF), Rivand (RF), Neyshabur (NF), and Binalud (BF) faults, for
603 which high strain-based activity rates have been seen (see Figure 5 for the fault locations).

604 The EMME is the most up-to-date regional model, in which the whole Iranian Plateau
605 and both geological data and observed seismicity have been used (Danciu et al. 2018,
606 Şeşetyan et al. 2018). These facts make the EMME a decant candidate for comparison
607 purposes. To illustrate the spatial pattern of the differences between DBHM and EMME
608 models for various POEs, the ratio of the mean PGA value from DBHM to EMME is
609 calculated and presented in the form of the natural logarithm (Figures 9 (a) and 9 (b)). For
610 Azerbaijan, the average values of PGA are 30% and 15% higher than the PGA values derived
611 from EMME for 10% and 2% POEs in 50 years, respectively, and for Alborz, the average
612 values are 22% and 3% higher than the PGA derived from EMME for 10% and 2% POEs,

613 respectively. For large parts of the Alborz and Azerbaijan provinces, where earthquakes with
614 moderate-to-large recurrence times happen, the PGA values estimated from DBHM are
615 higher than the corresponding ones from EMME. According to Berberian and Yeats (1999),
616 the Alborz and Kopeh Dagh provinces are characterized by large-magnitude shallow
617 earthquakes separated by quiescent periods of 3000 to 5000 years on frontal reverse faults
618 and some strike-slip faults. In contrast, the Zagros province is characterized by rapid uplift,
619 high seismicity, and moderate-magnitude earthquakes on several blind reverse faults with
620 historical recurrence intervals of 300 to 500 years (Berberian and Yeats 1999).

621 In the Kopeh Dagh province, also the average PGA values are 23% and 6% higher than
622 the PGA values derived from EMME for 10% and 2% POEs, respectively. Although our
623 estimates of PGA for most parts of the Iranian Plateau (e.g., Azerbaijan, Alborz, Kopeh Dagh
624 provinces) are higher than EMME model estimates, estimates from the EMME for the Zagros
625 province on average are 32% and 38% higher than the values derived from DBHM for 10%
626 and 2% POEs, respectively. It is worth mentioning that the EMME source model consists of
627 two layers of the seismogenic sources (i.e., shallow sources and deep sources with a
628 hypocentral depth of higher than 50 km) in the Zagros province, and two GMPEs (i.e.,
629 Youngs et al. (1997) and Lin and Lee (2008)) developed for subduction zones with equal
630 weights are assigned to deep sources. These GMPEs provide higher PGA than our considered
631 GMPEs.

632 For the Eastern Iran province, on average the PGA values estimated based on DBHM are
633 28% and 7% higher than PGA values derived from EMME for 10% and 2% POEs,
634 respectively. The main reason for these differences could be the lack of enough data for
635 large-magnitude events since Central and Eastern Iran are characterized by long recurrence
636 times. For the Central Iran province, on average the PGA values which are estimated based
637 on the DBHM model are 12% and 1%, higher than PGA values derived from the EMME

638 model for 10% and 2% POEs in 50 years, respectively. The main reason for these lower
639 differences for Central Iran could be justified by the presence of Zagros seismogenic sources
640 for which the EMME model is provided with high hazard levels.

641

642 **6.2. Hazard curves**

643 In order to have a full picture of the annual probabilities of exceedance, we also show PGA
644 hazard curves for important cities in Iran (see Figure 10) by picking up the POEs for 16
645 hazard levels between 0.001g - 3.5 g in 50 years. These cities are located in different
646 seismotectonic provinces as follows: Tehran in the Alborz province, Tabriz in the Azerbaijan
647 province, Kermanshah, Ahvaz, Shiraz, and Bandar Abbas in the Zagros province, Kerman in
648 Eastern Iran, Isfahan in Central Iran and Bojnurd and Mashhad in the Kopeh Dagh province.
649 In the following, we made a comparison between the DBHM hazard values and results of
650 available seismic hazard models for different regions of the Iranian Plateau.

651 Two catalog-based seismic hazard models are provided for Iran using the smoothed
652 seismicity approach. The first one is Khodaverdian et al. (2016b) (Kh16), which provided for
653 the whole Iranian Plateau and the second one is Khoshnevis et al. (2017) (Kh17), which
654 provided for the northern part of Iran including Azerbaijan, Alborz, Kopeh Dagh, the
655 northern part of Zagros, and the northern part of the Central Iran and Eastern Iran provinces.
656 In both models, all the observed earthquakes are distributed in the area sources and are not
657 assigned to specific faults. Hence, the effect of fault proximity is not seen in their hazard
658 assessment results. Moreover, two hazard models are available for Tehran and surrounding
659 areas: (1) Zafarani et al. (2017) (Za17), in which seismic hazard model is provided based on
660 the characteristic earthquake model, and (2) Jalalalhosseini et al. (2018) (Ja18), providing a
661 time-dependent hazard model. Shabani and Mirzaei (2007) (Sh07) is a catalog-based PSHA
662 model for the Kermanshah region. Eskandarinejad et al. (2018) (Es18) includes both

663 traditional catalog-based and Monte-Carlo simulation-based PSHA for Shiraz city. The 16%,
664 50%, mean, and 84% quantile curves and results of the above-mentioned models for selected
665 cities are shown in Figure 10.

666 The results of the mentioned models for Tehran are shown in Figure 10 (a). The PGA
667 values derived from DBHM are 0.38 g and 0.63 g for 10% and 2% POEs in 50 years,
668 respectively. The PGA values derived from EMME are 0.45 g and 0.87 g for 10% and 2%
669 POEs, respectively. The differences between PGA values derived from DBHM and EMME
670 for Tehran city are lower than the differences we have seen for the large portion of sites in the
671 Alborz province. The main reason is that, for the region close to Tehran, the geological
672 properties (e.g., geological slip rates) of the faults near to the city are studied in various
673 researches (Ritz et al. 2003, Nazari et al. 2009) and implemented in EMME. In general, we
674 may expect the hazard results are in good agreement with our prediction if a geological
675 investigation of the faults near a site is implemented in the hazard model. However, estimates
676 of Kh16 (i.e., 0.22 g and 0.45 g for 10% and 2% POEs, respectively), Za17(i.e., 0.28 g and
677 0.54 g), Ja18 (i.e., 0.29 g and 0.56 g), Kh17 (i.e., 0.31 g and 0.53 g), in which only the
678 catalog of observed earthquakes are used, are less than DBHM results. That could be justified
679 by the presence of well-known active faults nearby Tehran (e.g., North Tehran (NTF1) and
680 Mosha (MF) faults) while the observed earthquakes are assigned to a wide area instead of
681 near-fault zones, and consequently smoothed seismicity hazard models (i.e., Kh16 and Kh17)
682 resulted in lower PGA values.

683 Estimated PGA values for Tabriz city (i.e., 0.57 g and 0.91 g for 10% and 2% POEs in
684 50 years, respectively) are close to results of the EMME model (i.e., 0.61 g and 1.10 g)
685 (Figure 10 (b)). The geological slip rate of the active faults nearby Tabriz city is studied in
686 various researches (Rizza et al. 2013) and is implemented in the EMME project model, which
687 is the main reason for this consistency. Estimates of Kh16 (i.e., 0.22 g and 0.46 g) and Kh17

688 (i.e., 0.35 g and 0.61 g) are less than the values of DBHM and EMME models. The reason is
689 the lack of a fault-based approach in these models; mainly the North Tabriz fault (NTF2),
690 which is located in the proximity of the city, is not included in both Kh16 and Kh17 models.

691 For Ahvaz city in the Zagros province, the PGA values derived from the DBHM model
692 for 10% and 2% POEs in 50 years are 0.21 g and 0.39 g, respectively, and are in good
693 agreement with Kh16 estimated values (i.e., 0.21 g and 0.41 g) (Figure 10 (c)). It shows that
694 distributed seismicity source is a plausible assumption for that region. This fact could be
695 supported by the presence of several hidden secondary/minor faults located around the city of
696 Ahvaz (Berberian 1995, Abedi and Oskooi 2015, SABOUR et al. 2015). For Kermanshah
697 city, our estimates (i.e., 0.32 g and 0.55 g) are higher than the results of the Kh16 model (i.e.,
698 0.22 g and 0.44 g) (Figure 10 (d)). Also, Sh07 has reported a PGA of 0.2 g for 10% POE for
699 Kermanshah which is lower than the result of the DBHM. For Shiraz, the estimate of Es18 is
700 ~0.22 g for 10% POE, which is close to the DBHM's result (i.e., 0.24 g) (Figure 10 (f)). The
701 discrepancy between PGA values derived from deformation-based and catalog-based models
702 for all selected cities located in the Zagros seismotectonic province (i.e., Ahvaz, Kermanshah,
703 Bandar Abbas, and Shiraz) is lower than the discrepancy for cities in other provinces, which
704 could be justified by the relatively short recurrence times of earthquakes that occur in the
705 Zagros (also see Figure 10 (e)). Also, for all selected cities located in the Zagros, we have
706 seen that our results are lower than EMME's estimates, which is supporting the pattern we
707 mentioned in section 6.1.

708 Bojnurd and Mashhad are two selected cities in the Kopeh Dagh seismotectonic province.
709 The estimated PGA values for Bojnurd (i.e., 0.40 g and 0.7 g for 10% and 2% POEs in
710 50 years, respectively) are more than the values derived from the EMME (i.e., 0.36 g and
711 0.69 g) and Kh16 models (i.e., 0.27 g and 0.54 g) (Figure 10 (g)). Moreover, for Mashhad,
712 the estimated PGA values based on the DBHM (i.e., 0.37 g and 0.64 g) are more than the

values derived from the EMME model (i.e., 0.21 g and 0.44 g) and Kh16 (i.e., 0.15 g and 0.34 g) (Figure 10 (h)). As mentioned in section 6.1, high activity rates based on strain rates have been seen for the strip, which is extended from the east of the Alborz to Mashhad city. Kh17 estimated 0.22 g, and 0.39 g for 10% and 2% POEs, respectively, which are close to PGA values from the EMME model, as both models are based on observed seismicity.

Our PGA values for Isfahan city in Central Iran (i.e., 0.17 g, and 0.31 g for 10% and 2% POEs in 50 years, respectively) are close to the PGA values derived from EMME (i.e., 0.15 g and 0.43 g) and Kh16's estimates (i.e., 0.14 g and 0.32 g) (Figure 10 (i)). Isfahan is located in an aseismic block of central Iran, where low strain rates are observed (Figure 2a). Therefore, for Isfahan, we expect the differences between the deformation-based and catalog-based results are less in comparison to other regions in this province, which are close to the active faults (e.g., Dehshir (DF), Kashan (KF), Zefreh (ZF), and Indes (IF)).

Figure 10 (j) shows that our PGA estimates for Kerman city in Eastern Iran are 0.35 g and 0.61 g for 10% and 2% POEs in 50 years, respectively, and more than the estimates of EMME (i.e., 0.25 g and 0.47 g). Kh16's estimates (i.e., 0.26 g and 0.5 g) are close to the estimates of EMME. Earthquakes in Eastern Iran seismotectonic province almost occur with long recurrence intervals; therefore, catalog-based seismic hazard might underestimate the possible expected PGA.

We also build another version of the DBHM model by employing GMPEs from the EMME model to investigate the effect of GMPEs. Hazard analyses are carried out for the cities where significant discrepancies in the outcomes of the DBHM and EMME models have been observed. As shown in Figure 11, the application of the EMME's GMPE does not lead to substantial variations in hazard curves – the estimated PGA for 475 years return period are changed less than 20%; it can be interpreted that a majority of the difference (more than 80%

737 for 475 years return period) between DBHM and EMME models is due to differences in the
738 source models, particularly earthquake occurrence rates.

739

740 ## 7. Conclusions

741 Several investigations have shown that available short instrumental earthquake catalogs or
742 limited historical evidence may not be enough for estimation of the long-term earthquake
743 occurrences rate, especially for an area that is characterized by large-magnitude earthquakes.
744 Catalog-based seismic hazard assessment, consequently, could be challenging. Deformation
745 data (i.e., GPS velocities and geological fault slip rates) could be used for the enrichment of a
746 regional seismic hazard model when it is combined with seismic data from earthquake
747 catalogs.

748 We used a methodology to estimate earthquake occurrence rates from strain rates and
749 implemented it by using the outcome of the comprehensive deformation model of the Iranian
750 Plateau. The comparison between the catalog-based long-term earthquake occurrence rates
751 and deformation-based occurrence rates shows the lowest amount of $\lambda_4^D / \lambda_4^C$ (i.e., 1.21) is
752 observed in the Zagros province, where earthquakes with relatively short recurrence times
753 occur. The maximum amount of $\lambda_4^D / \lambda_4^C$ (i.e., 8.88) is observed for Eastern Iran, where
754 large-magnitude earthquakes occur with long recurrence times. Sensitivity analysis shows
755 that the variation of seismogenic layer thickness has a considerable effect on driving activity
756 rate from strain rate, and it could not be ignored compared with the uncertainties of the
757 seismicity parameters.

758 We generated square area sources, for a grid with the same spacing of the strain rate
759 model $(0.2^o \times 0.2^o)$ covering the whole Plateau. The seismicity parameters (e.g., deformation-

760 based activity rates, β and m_{max}), evaluated based on the proposed methodology, are
761 assigned to each $0.2^{o} \times 0.2^{o}$ area source. The seismotectonic characteristics of each area
762 source are evaluated based on the characteristics of the nearest fault and the seismotectonic
763 map of the Iranian Plateau. Logic trees of the hypocenter depths, seismicity parameters, and
764 GMPEs are employed in an attempt to capture their uncertainties.

765 We estimate PGA hazard maps at 10% and 2% POEs in 50 years. The highest levels of
766 hazard are found in the Azerbaijan and Alborz seismic provinces, where the highest value of
767 strain rates is also located. Generally, the comparison between the DBHM and catalog-based
768 models shows that catalog-based PGA values are lower than deformation-based PGA values
769 for most areas of the Iranian Plateau, which could be justified by the lack of recorded large-
770 magnitude earthquakes due to their long-term recurrence times. Specifically, the comparison
771 between the EMME and DBHM can be summarised in four points: (1) For all provinces
772 except the Zagros, the DBHM resulted in higher PGA values than EMME. In the EMME
773 model, GMPEs, which resulted in high PGA, are used for Zagros. (2) There are up to ~30%
774 differences between the spatial average of PGA values with 10% POE in 50 years, which
775 derived from EMME and DBHM for seismotectonic provinces of the Iranian Plateau. (3) For
776 the city of Tehran and Tabriz, the results of the EMME and DBHM models are in good
777 agreement. The geological properties (i.e., slip rates) of active faults near these cities are
778 implemented in the EMME model and the consequences of lack of a long-term catalog have
779 been reduced. Therefore, we expect catalog-based hazard models have a better estimate if the
780 geological properties of the active faults near a site are implemented in a catalog-based
781 model. (4) A majority of the difference between DBHM and EMME models is due to
782 differences in the source models, particularly earthquake occurrence rates.

783

Acknowledgments

We thank the continuing support of the International Institute of Earthquake Engineering and Seismology during this research, in the framework of the Probabilities of Earthquake Ruptures in Iran (PERSIA).

References

Abdollahzadeh, G., L. Khanmohammadi and F. Zahedi Tajrishi (2014a). "Modified probabilistic approach for seismic hazard zoning of Golestan region, Iran." European journal of environmental and civil engineering **18**(4): 427-456.

Abdollahzadeh, G., M. Sazjini, M. Shahaky, F. Z. Tajrishi and L. Khanmohammadi (2014b). "Considering potential seismic sources in earthquake hazard assessment for Northern Iran." Journal of seismology **18**(3): 357-369.

Abedi, M. and B. Oskooi (2015). "A combined magnetometry and gravity study across Zagros orogeny in Iran." Tectonophysics **664**: 164-175.

Abrahamson, N. A., W. J. Silva and R. Kamai (2014). "Summary of the ASK14 ground motion relation for active crustal regions." Earthquake Spectra **30**(3): 1025-1055.

Aghanabati, A. (2004). "Geology of Iran: Geological Survey of Iran, 600."

Allen, M. B., M. Kheirkhah, M. H. Emami and S. J. Jones (2011). "Right-lateral shear across Iran and kinematic change in the Arabia—Eurasia collision zone." Geophysical Journal International **184**(2): 555-574.

Ambraseys, N. and C. Melville (1982). "A History of Persian Earthquakes Cambridge Univ." Press, New York.

Anderson, J. G. and J. E. Luco (1983). "Consequences of slip rate constraints on earthquake occurrence relations." Bulletin of the Seismological Society of America **73**(2): 471-496.

Ansari, A., A. Noorzad and H. Zafarani (2009). "Clustering analysis of the seismic catalog of Iran." Computers & Geosciences **35**(3): 475-486.

Bachmanov, D., V. Trifonov, K. T. Hessami, A. Kozhurin, T. Ivanova, E. Rogozhin, M. Hademi and F. Jamali (2004). "Active faults in the Zagros and central Iran." Tectonophysics **380**(3-4): 221-241.

Bayer, R., J. Chery, M. Tatar, P. Vernant, M. Abbassi, F. Masson, F. Nilforoushan, E. Doerflinger, V. Regard and O. Bellier (2006). "Active deformation in Zagros—Makran transition zone inferred from GPS measurements." Geophysical Journal International **165**(1): 373-381.

Beauval, C., P.-Y. Bard, S. Hainzl and P. Gueguen (2008). "Can strong-motion observations be used to constrain probabilistic seismic-hazard estimates?" Bulletin of the Seismological Society of America **98**(2): 509-520.

Berberian, M. (1976a). "CONTRIBUTION TO THE SEISMOTECTONICS OF IRAN. II."

Berberian, M. (1976b). Seismotectonic map of Iran, scale 1/2,500,000. Contribution ot the Seismotectonics of Iran (Part II). **39:** 516.

Berberian, M. (1981). "Active faulting and tectonics of Iran." Zagros-Hindu Kush-Himalaya Geodynamic Evolution **3**: 33-69.

Berberian, M. (1994). "Natural hazards and the first earthquake catalogue of Iran. Volume 1: Historical hazards in Iran prior to 1900." Int. Inst. Earthquake Engineering and Seismology, Tehran: 603pp.

Berberian, M. (1995). "Master “blind” thrust faults hidden under the Zagros folds: active basement tectonics and surface morphotectonics." Tectonophysics **241**(3-4): 193-224.

Berberian, M. (2014). Patterns of historical earthquake ruptures on the Iranian plateau. Developments in Earth Surface Processes, Elsevier. **17:** 439-518.

Berberian, M., C. A. Petrie, D. Potts, A. A. Chaverdi, A. Dusting, A. S. Zarchi, L. WEEKS, P. Ghassemi and R. Noruzi (2014). "Archaeoseismicity of the Mounds and Monuments Along the Kazerun Fault (western Zagros, Sw Iranian Plateau) Since the Chalcolithic Period." Iranica Antiqua **49**: 1-81.

Berberian, M. and R. S. Yeats (1999). "Patterns of historical earthquake rupture in the Iranian Plateau." Bulletin of the Seismological society of America **89**(1): 120-139.

Berberian, M. and R. S. Yeats (2001). "Contribution of archaeological data to studies of earthquake history in the Iranian Plateau." Journal of Structural Geology **23**(2): 563-584.

841 Bird, P. and M. M. Carafa (2016). "Improving deformation models by discounting transient signals in
842 geodetic data: 1. Concept and synthetic examples." Journal of Geophysical Research: Solid Earth
843 **121**(7): 5538-5556.
844 Bird, P. and Y. Y. Kagan (2004). "Plate-tectonic analysis of shallow seismicity: Apparent boundary
845 width, beta, corner magnitude, coupled lithosphere thickness, and coupling in seven tectonic
846 settings." Bulletin of the Seismological Society of America **94**(6): 2380-2399.
847 Bommer, J. J. (2012). "Challenges of building logic trees for probabilistic seismic hazard analysis."
848 Earthquake Spectra **28**(4): 1723-1735.
849 Bommer, J. J. and N. A. Abrahamson (2006). "Why do modern probabilistic seismic-hazard analyses
850 often lead to increased hazard estimates?" Bulletin of the Seismological Society of America **96**(6):
851 1967-1977.
852 Bommer, J. J., J. Douglas, F. Scherbaum, F. Cotton, H. Bungum and D. Fäh (2010). "On the selection of
853 ground-motion prediction equations for seismic hazard analysis." Seismological Research Letters
854 **81**(5): 783-793.
855 Boore, D. M. (2010). "Orientation-independent, nongeometric-mean measures of seismic intensity
856 from two horizontal components of motion." Bulletin of the Seismological Society of America **100**(4):
857 1830-1835.
858 Bozorgnia, Y., N. A. Abrahamson, L. A. Atik, T. D. Ancheta, G. M. Atkinson, J. W. Baker, A. Baltay, D.
859 M. Boore, K. W. Campbell and B. S.-J. Chiou (2014). "NGA-West2 research project." Earthquake
860 Spectra **30**(3): 973-987.
861 Bungum, H., C. D. Lindholm and A. K. Mahajan (2017). "Earthquake recurrence in NW and central
862 Himalaya." Journal of Asian Earth Sciences **138**: 25-37.
863 Carafa, M. M. and P. Bird (2016). "Improving deformation models by discounting transient signals in
864 geodetic data: 2. Geodetic data, stress directions, and long-term strain rates in Italy." Journal of
865 Geophysical Research: Solid Earth **121**(7): 5557-5575.
866 Copley, A. and J. Jackson (2006). "Active tectonics of the Turkish-Iranian plateau." Tectonics **25**(6).
867 Cotton, F., F. Scherbaum, J. J. Bommer and H. Bungum (2006). "Criteria for selecting and adjusting
868 ground-motion models for specific target regions: Application to central Europe and rock sites."
869 Journal of Seismology **10**(2): 137.
870 Danciu, L., K. Şeşetyan, M. Demircioglu, L. Gülen, M. Zare, R. Basili, A. Elias, S. Adamia, N. Tsereteli
871 and H. Yalçın (2018). "The 2014 earthquake model of the middle east: seismogenic sources." Bulletin
872 of Earthquake Engineering **16**(8): 3465-3496.
873 Djamour, Y., P. Vernant, H. R. Nankali and F. Tavakoli (2011). "NW Iran-eastern Turkey present-day
874 kinematics: results from the Iranian permanent GPS network." Earth and Planetary Science Letters
875 **307**(1-2): 27-34.
876 Engdahl, E. R., J. A. Jackson, S. C. Myers, E. A. Bergman and K. Priestley (2006). "Relocation and
877 assessment of seismicity in the Iran region." Geophysical Journal International **167**(2): 761-778.
878 Eskandarinejad, A., H. Zafarani and M. Jahanandish (2018). "Comparison of conventional and Monte
879 Carlo simulation-based probabilistic seismic hazard analyses for Shiraz city, southern Iran." Journal of
880 Seismology **22**(6): 1629-1643.
881 Field, E. H. (2015). UCERF3: A new earthquake forecast for California's complex fault system, US
882 Geological Survey.
883 Field, E. H., R. J. Arrowsmith, G. P. Biasi, P. Bird, T. E. Dawson, K. R. Felzer, D. D. Jackson, K. M.
884 Johnson, T. H. Jordan and C. Madden (2014). "Uniform California Earthquake Rupture Forecast,
885 Version 3 (UCERF3)—The Time-Independent Model." Bulletin of the Seismological Society of America
886 **104**(3): 1122-1180.
887 Field, E. H., G. P. Biasi, P. Bird, T. E. Dawson, K. R. Felzer, D. D. Jackson, K. M. Johnson, T. H. Jordan, C.
888 Madden and A. J. Michael (2015). "Long-term time-dependent probabilities for the third Uniform
889 California Earthquake Rupture Forecast (UCERF3)." Bulletin of the Seismological Society of America
890 **105**(2A): 511-543.

Field, E. H., T. E. Dawson, K. R. Felzer, A. D. Frankel, V. Gupta, T. H. Jordan, T. Parsons, M. D. Petersen, R. S. Stein and R. Weldon (2009). "Uniform California earthquake rupture forecast, version 2 (UCERF 2)." Bulletin of the Seismological Society of America **99**(4): 2053-2107.

Foroutan, M., B. Meyer, M. Sébrier, H. Nazari, A. Murray, K. Le Dortz, M. Shokri, M. Arnold, G. Aumaître and D. Bourlès (2014). "Late Pleistocene-Holocene right slip rate and paleoseismology of the Nayband fault, western margin of the Lut block, Iran." Journal of Geophysical Research: Solid Earth **119**(4): 3517-3560.

Foroutan, M., M. Sébrier, H. Nazari, B. Meyer, M. Fattahi, A. Rashidi, K. Le Dortz and M. Bateman (2012). "New evidence for large earthquakes on the Central Iran plateau: palaeoseismology of the Anar fault." Geophysical Journal International **189**(1): 6-18.

Gardner, J. and L. Knopoff (1974). "Is the sequence of earthquakes in Southern California, with aftershocks removed, Poissonian?" Bulletin of the seismological society of America **64**(5): 1363-1367.

Ghodrati Amiri, G., R. Motamed and H. Rabet Es-Haghi (2003). "Seismic hazard assessment of metropolitan Tehran, Iran." Journal of Earthquake Engineering **7**(3): 347-372.

Godano, C. and F. Pingue (2000). "Is the seismic moment–frequency relation universal?" Geophysical Journal International **142**(1): 193-198.

Hanks, T. C. and H. Kanamori (1979). "A moment magnitude scale." J. Geophys. Res. **84**: 2348-2350.

Hessami, K., F. Mobayyen and H. Tabassi (2013). "The map of active faults of Iran." International institute of earthquake engineering and seismology Tehran.

Hessami, K., F. Nilforoushan and C. J. Talbot (2006). "Active deformation within the Zagros Mountains deduced from GPS measurements." Journal of the Geological Society **163**(1): 143-148.

Hong, Y., C. Guoguang and Z. Qing (1996). Study on the intraplate potential seismic sources. International conference on seismic zonation.

Idriss, I. (2014). "An NGA-West2 empirical model for estimating the horizontal spectral values generated by shallow crustal earthquakes." Earthquake Spectra **30**(3): 1155-1177.

Jackson, J. (1992). "Partitioning of strike-slip and convergent motion between Eurasia and Arabia in eastern Turkey and the Caucasus." Journal of Geophysical Research: Solid Earth **97**(B9): 12471-12479.

Jackson, J., J. Haines and W. Holt (1995). "The accommodation of Arabia-Eurasia plate convergence in Iran." Journal of Geophysical Research: Solid Earth **100**(B8): 15205-15219.

Jackson, J. and D. McKenzie (1984). "Active tectonics of the Alpine—Himalayan Belt between western Turkey and Pakistan." Geophysical Journal International **77**(1): 185-264.

Jalalalhosseini, S. M., H. Zafarani and M. Zare (2018). "Time-dependent seismic hazard analysis for the Greater Tehran and surrounding areas." Journal of Seismology **22**(1): 187-215.

Kalaneh, S. and M. Agh-Atabai (2016). "Spatial variation of earthquake hazard parameters in the Zagros fold and thrust belt, SW Iran." Natural Hazards **82**(2): 933-946.

Kale, Ö., S. Akkar, A. Ansari and H. Hamzehloo (2015). "A ground-motion predictive model for Iran and Turkey for horizontal PGA, PGV, and 5% damped response spectrum: Investigation of possible regional effects." Bulletin of the Seismological Society of America **105**(2A): 963-980.

Karakhanian, A. S., V. G. Trifonov, H. Philip, A. Avagyan, K. Hessami, F. Jamali, M. S. Bayraktutan, H. Bagdassarian, S. Arakelian and V. Davtian (2004). "Active faulting and natural hazards in Armenia, eastern Turkey and northwestern Iran." Tectonophysics **380**(3-4): 189-219.

Khodaverdian, A., H. Zafarani and M. Rahimian (2015). "Long term fault slip rates, distributed deformation rates and forecast of seismicity in the Iranian Plateau." Tectonics **34**(10): 2190-2220.

Khodaverdian, A., H. Zafarani and M. Rahimian (2016a). "Using a physics-based earthquake simulator to evaluate seismic hazard in NW Iran." Geophysical Journal International **206**(1): 379-394.

Khodaverdian, A., H. Zafarani, M. Rahimian and V. Dehnamaki (2016b). "Seismicity Parameters and Spatially Smoothed Seismicity Model for Iran." Bulletin of the Seismological Society of America **106**(3): 1133-1150.

941 Khodaverdian, A., H. Zafarani, K. Schultz and M. Rahimian (2016c). "Recurrence time distributions of
942 large earthquakes in Eastern Iran." Bulletin of the Seismological Society of America **106**(6): 2624-
943 2639.
944 Khoshnevis, N., R. Taborda, S. Azizzadeh-Roodpish and C. H. Cramer (2017). "Seismic hazard
945 estimation of northern Iran using smoothed seismicity." Journal of Seismology **21**(4): 941-964.
946 Kijko, A., A. Smit and M. A. Sellevoll (2016). "Estimation of earthquake hazard parameters from
947 incomplete data files. Part III. Incorporation of uncertainty of earthquake-occurrence model."
948 Bulletin of the Seismological Society of America **106**(3): 1210-1222.
949 Kreemer, C., G. Blewitt and E. C. Klein (2014). "A geodetic plate motion and Global Strain Rate
950 Model." Geochemistry, Geophysics, Geosystems **15**(10): 3849-3889.
951 Le Dortz, K., B. Meyer, M. Sébrier, R. Braucher, H. Nazari, L. Benedetti, M. Fattahi, D. Bourlès, M.
952 Foroutan and L. Siame (2011). "Dating inset terraces and offset fans along the Dehshir Fault (Iran)
953 combining cosmogenic and OSL methods." Geophysical Journal International **185**(3): 1147-1174.
954 Le Dortz, K., B. Meyer, M. Sébrier, H. Nazari, R. Braucher, M. Fattahi, L. Benedetti, M. Foroutan, L.
955 Siame and D. Bourlès (2009). "Holocene right-slip rate determined by cosmogenic and OSL dating on
956 the Anar fault, Central Iran." Geophysical Journal International **179**(2): 700-710.
957 Lin, P.-S. and C.-T. Lee (2008). "Ground-motion attenuation relationships for subduction-zone
958 earthquakes in northeastern Taiwan." Bulletin of the Seismological Society of America **98**(1): 220-
959 240.
960 Maggi, A., J. Jackson, K. Priestley and C. Baker (2000). "A re-assessment of focal depth distributions
961 in southern Iran, the Tien Shan and northern India: Do earthquakes really occur in the continental
962 mantle?" Geophysical Journal International **143**(3): 629-661.
963 Masson, F., M. Anvari, Y. Djamour, A. Walpersdorf, F. Tavakoli, M. Daignières, H. Nankali and S. Van
964 Gorp (2007). "Large-scale velocity field and strain tensor in Iran inferred from GPS measurements:
965 new insight for the present-day deformation pattern within NE Iran." Geophysical Journal
966 International **170**(1): 436-440.
967 Masson, F., J. Chéry, D. Hatzfeld, J. Martinod, P. Vernant, F. Tavakoli and M. Ghafory-Ashtiani (2005).
968 "Seismic versus aseismic deformation in Iran inferred from earthquakes and geodetic data."
969 Geophysical Journal International **160**(1): 217-226.
970 Masson, F., Y. Djamour, S. Van Gorp, J. Chéry, M. Tatar, F. Tavakoli, H. Nankali and P. Vernant (2006).
971 "Extension in NW Iran driven by the motion of the South Caspian Basin." Earth and Planetary Science
972 Letters **252**(1): 180-188.
973 Mazzotti, S., L. Leonard, J. Cassidy, G. Rogers and S. Halchuk (2011). "Seismic hazard in western
974 Canada from GPS strain rates versus earthquake catalog." Journal of Geophysical Research: Solid
975 Earth **116**(B12).
976 Mirzaei, N., G. Mengtan and C. Yuntai (1998). "Seismic source regionalization for seismic zoning of
977 Iran: major seismotectonic provinces." Journal of Earthquake Prediction Research **7**: 465-495.
978 Mooney, W. D., G. Laske and T. G. Masters (1998). "CRUST 5.1: A global crustal model at 5× 5."
979 Journal of Geophysical Research: Solid Earth **103**(B1): 727-747.
980 Mousavi-Bafrouei, S. H., N. Mirzaei and E. Shabani (2015). "A declustered earthquake catalog for the
981 Iranian Plateau." Annals of Geophysics **57**(6).
982 Mousavi, M., A. Ansari, H. Zafarani and A. Azarbakht (2012). "Selection of ground motion prediction
983 models for seismic hazard analysis in the Zagros region, Iran." Journal of Earthquake Engineering
984 **16**(8): 1184-1207.
985 Mousavi, Z., A. Walpersdorf, R. Walker, F. Tavakoli, E. Pathier, H. Nankali, F. Nilfouroushan and Y.
986 Djamour (2013). "Global Positioning System constraints on the active tectonics of NE Iran and the
987 South Caspian region." Earth and Planetary Science Letters **377**: 287-298.
988 Nazari, H. (2006). Analyse de la tectonique récente et active dans l'Alborz Central et la région de
989 Téhéran:«Approche morphotectonique et paléoseismologique», Université Montpellier II-Sciences
990 et Techniques du Languedoc.

991 Nazari, H., J.-F. Ritz, R. Salamati, A. Shafei, A. Ghassemi, J.-L. Michelot, M. Massault and M. Ghorashi
992 (2009). "Morphological and palaeoseismological analysis along the Taleghan fault (Central Alborz,
993 Iran)." Geophysical Journal International **178**(2): 1028-1041.
994 Nilforoushan, F., F. Masson, P. Vernant, C. Vigny, J. Martinod, M. Abbassi, H. Nankali, D. Hatzfeld, R.
995 Bayer and F. Tavakoli (2003). "GPS network monitors the Arabia-Eurasia collision deformation in
996 Iran." Journal of Geodesy **77**(7-8): 411-422.
997 Nowroozi, A. A. (1976). "Seismotectonic provinces of Iran." Bulletin of the Seismological Society of
998 America **66**(4): 1249-1276.
999 Pagani, M., D. Monelli, G. Weatherill, L. Danciu, H. Crowley, V. Silva, P. Henshaw, L. Butler, M.
1000 Nastasi and L. Panzeri (2014). "OpenQuake engine: An open hazard (and risk) software for the global
1001 earthquake model." Seismological Research Letters **85**(3): 692-702.
1002 Petersen, M. D., T. Cao, K. W. Campbell and A. D. Frankel (2007). "Time-independent and time-
1003 dependent seismic hazard assessment for the State of California: Uniform California Earthquake
1004 Rupture Forecast Model 1.0." Seismological Research Letters **78**(1): 99-109.
1005 Rajendran, C., K. Rajendran, J. Sanwal and M. Sandiford (2013). "Archeological and historical
1006 database on the medieval earthquakes of the central Himalaya: Ambiguities and inferences."
1007 Seismological Research Letters **84**(6): 1098-1108.
1008 Ritz, J., S. Balescu, S. Soleymani, M. Abbassi, H. Nazari, K. Feghhi, E. Shabanian, H. Tabassi, Y. Farbod
1009 and M. Lamothe (2003). Determining the long-term slip rate along the Mosha Fault, Central Alborz,
1010 Iran. Implications in terms of seismic activity. Proceeding of the 4th International Conference on
1011 Seismology and Earthquake Engeneering, Tehran, Iran.
1012 Ritz, J. F., H. Nazari, S. Balescu, M. Lamothe, R. Salamati, A. Ghassemi, A. Shafei, M. Ghorashi and A.
1013 Saidi (2012). "Paleoearthquakes of the past 30,000 years along the North Tehran Fault (Iran)."
1014 Journal of Geophysical Research: Solid Earth **117**(B6).
1015 Rizza, M., P. Vernant, J.-F. Ritz, M. Peyret, H. Nankali, H. Nazari, Y. Djamour, R. Salamati, F. Tavakoli
1016 and J. Chery (2013). "Morphotectonic and geodetic evidence for a constant slip-rate over the last 45
1017 kyr along the Tabriz fault (Iran)." Geophysical Journal International **193**(3): 1083-1094.
1018 SABOUR, N., M. R. GHASSEMI and B. OVEISI (2015). "STRUCTURAL MATURITY OF BLIND FAULTS IN
1019 ZAGROS FOLD AND THRUST BELT."
1020 Savage, J. and R. Simpson (1997). "Surface strain accumulation and the seismic moment tensor."
1021 Bulletin of the Seismological Society of America **87**(5): 1345-1353.
1022 Şeşetyan, K., L. Danciu, M. B. D. Tümsa, D. Giardini, M. Erdik, S. Akkar, L. Gülen, M. Zare, S. Adamia
1023 and A. Ansari (2018). "The 2014 seismic hazard model of the Middle East: overview and results."
1024 Bulletin of Earthquake Engineering **16**(8): 3535-3566.
1025 Shabani, E. and N. Mirzaei (2007). "Probabilistic seismic hazard assessment of the Kermanshah-
1026 Sanandaj region of Western Iran." Earthquake Spectra **23**(1): 175-197.
1027 Shabanian, E., L. Siame, O. Bellier, L. Benedetti and M. R. Abbassi (2009). "Quaternary slip rates
1028 along the northeastern boundary of the Arabia-Eurasia collision zone (Kopeh Dagh Mountains,
1029 Northeast Iran)." Geophysical Journal International **178**(2): 1055-1077.
1030 Shahvar, M. P., M. Zare and S. Castellaro (2013). "A unified seismic catalog for the Iranian plateau
1031 (1900–2011)." Seismological Research Letters **84**(2): 233-249.
1032 Shoja–Taheri, J., S. Naserieh and G. Hadi (2010). "A test of the applicability of NGA models to the
1033 strong ground-motion data in the Iranian plateau." Journal of Earthquake Engineering **14**(2): 278-
1034 292.
1035 Srivastava, H., M. Verma, B. Bansal and A. K. Sutar (2015). "Discriminatory characteristics of seismic
1036 gaps in Himalaya." Geomatics, Natural Hazards and Risk **6**(3): 224-242.
1037 Stein, R. S. (1999). "The role of stress transfer in earthquake occurrence." Nature **402**(6762): 605.
1038 Stepp, J. (1972). Analysis of completeness of the earthquake sample in the Puget Sound area and its
1039 effect on statistical estimates of earthquake hazard. Proc. of the 1st Int. Conf. on Microzonazion,
1040 Seattle.
1041 StScklin, J. (1968). "Structural history and tectonics of Iran." AAPG Bull **52**(7): 1229-1258.

Takin, M. (1972). "Iranian geology and continental drift in the Middle East." Nature **235**(5334): 147.
Talebian, M. and J. Jackson (2004). "A reappraisal of earthquake focal mechanisms and active shortening in the Zagros mountains of Iran." Geophysical Journal International **156**(3): 506-526.
Tatar, M., D. Hatzfeld, J. Martinod, A. Walpersdorf, M. Ghafori-Ashtiany and J. Chéry (2002). "The present-day deformation of the central Zagros from GPS measurements." Geophysical research letters **29**(19): 33-31-33-34.
Tavakoli, F., A. Walpersdorf, C. Authemayou, H. Nankali, D. Hatzfeld, M. Tatar, Y. Djamour, F. Nilforoushan and N. Cotte (2008). "Distribution of the right-lateral strike–slip motion from the Main Recent Fault to the Kazerun Fault System (Zagros, Iran): Evidence from present-day GPS velocities." Earth and Planetary Science Letters **275**(3-4): 342-347.
Vernant, P., F. Nilforoushan, J. Chery, R. Bayer, Y. Djamour, F. Masson, H. Nankali, J.-F. Ritz, M. Sedighi and F. Tavakoli (2004a). "Deciphering oblique shortening of central Alborz in Iran using geodetic data." Earth and Planetary Science Letters **223**(1-2): 177-185.
Vernant, P., F. Nilforoushan, D. Hatzfeld, M. Abbassi, C. Vigny, F. Masson, H. Nankali, J. Martinod, A. Ashtiani and R. Bayer (2004b). "Present-day crustal deformation and plate kinematics in the Middle East constrained by GPS measurements in Iran and northern Oman." Geophysical Journal International **157**(1): 381-398.
Walker, R. and J. Jackson (2004). "Active tectonics and late Cenozoic strain distribution in central and eastern Iran." Tectonics **23**(5).
Walker, R., J. Jackson and C. Baker (2004). "Active faulting and seismicity of the Dasht-e-Bayaz region, eastern Iran." Geophysical Journal International **157**(1): 265-282.
Walker, R., M. Talebian, R. Sloan, A. Rasheedi, M. Fattahi and C. Bryant (2010). "Holocene slip-rate on the Gowk strike-slip fault and implications for the distribution of tectonic strain in eastern Iran." Geophysical Journal International **181**(1): 221-228.
Walpersdorf, A., D. Hatzfeld, H. Nankali, F. Tavakoli, F. Nilforoushan, M. Tatar, P. Vernant, J. Chéry and F. Masson (2006). "Difference in the GPS deformation pattern of North and Central Zagros (Iran)." Geophysical Journal International **167**(3): 1077-1088.
Walpersdorf, A., I. Manighetti, Z. Mousavi, F. Tavakoli, M. Vergnolle, A. Jadidi, D. Hatzfeld, A. Aghamohammadi, A. Bigot and Y. Djamour (2014). "Present-day kinematics and fault slip rates in eastern Iran, derived from 11 years of GPS data." Journal of Geophysical Research: Solid Earth **119**(2): 1359-1383.
Ward, S. N. (1998). "On the consistency of earthquake moment rates, geological fault data, and space geodetic strain: the United States." Geophysical Journal International **134**(1): 172-186.
Ward, S. N. (2007). "Methods for evaluating earthquake potential and likelihood in and around California." Seismological Research Letters **78**(1): 121-133.
Wiemer, S. and M. Wyss (2000). "Minimum magnitude of completeness in earthquake catalogs: Examples from Alaska, the western United States, and Japan." Bulletin of the Seismological Society of America **90**(4): 859-869.
Yamini-Fard, F., D. Hatzfeld, M. Tatar and M. Mokhtari (2006). "Microearthquake seismicity at the intersection between the Kazerun fault and the Main Recent Fault (Zagros, Iran)." Geophysical Journal International **166**(1): 186-196.
Yaminifard, F., M. H. Sedghi, A. Gholamzadeh, M. Tatar and K. Hessami (2012). "Active faulting of the southeastern-most Zagros (Iran): Microearthquake seismicity and crustal structure." Journal of Geodynamics **55**: 56-65.
Youngs, R., S.-J. Chiou, W. Silva and J. Humphrey (1997). "Strong ground motion attenuation relationships for subduction zone earthquakes." Seismological Research Letters **68**(1): 58-73.
Zafarani, H. and A. Farhadi (2017). "Testing ground-motion prediction equations against small-to-moderate magnitude data in Iran." Bulletin of the Seismological Society of America **107**(2): 912-933.
Zafarani, H., B. Hajimohammadi and S. M. Jalalalhosseini (2017). "Earthquake hazard in the Tehran region based on the characteristic earthquake model." Journal of Earthquake Engineering: 1-27.

Zafarani, H., L. Luzi, G. Lanzano and M. Soghrat (2018). "Empirical equations for the prediction of PGA and pseudo spectral accelerations using Iranian strong-motion data." Journal of Seismology **22**(1): 263-285.
Zafarani, H. and M. Mousavi (2014). "Applicability of different ground-motion prediction models for northern Iran." Natural hazards **73**(3): 1199-1228.
Zare, M., H. Amini, P. Yazdi, K. Sesetyan, M. B. Demircioglu, D. Kalafat, M. Erdik, D. Giardini, M. A. Khan and N. Tsereteli (2014). "Recent developments of the Middle East catalog." Journal of seismology **18**(4): 749-772.
Zhao, J. X., J. Zhang, A. Asano, Y. Ohno, T. Oouchi, T. Takahashi, H. Ogawa, K. Irikura, H. K. Thio and P. G. Somerville (2006). "Attenuation relations of strong ground motion in Japan using site classification based on predominant period." Bulletin of the Seismological Society of America **96**(3): 898-913.

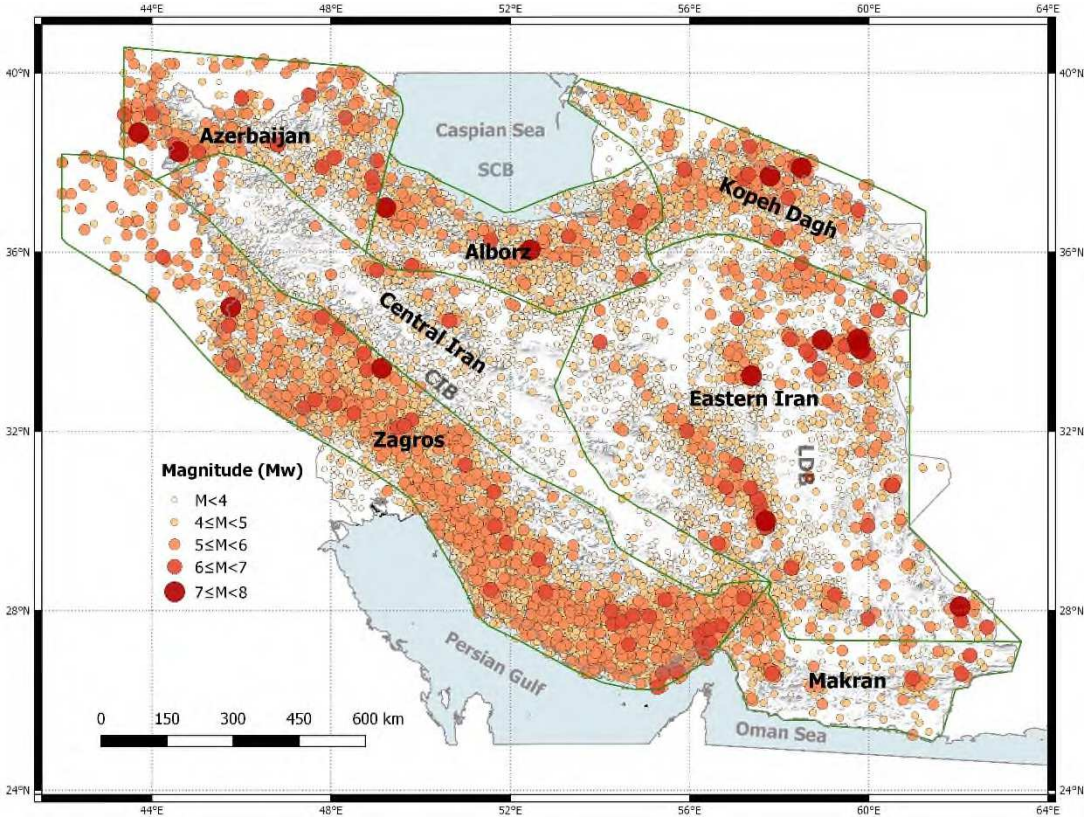

1117

1118 **Figure 1. Observed seismicity during 1900-2015 in the Iranian Plateau. Green lines**
1119 **show the border of seismotectonic provinces, adopted from Mirzaei et al. (1998)**

1120

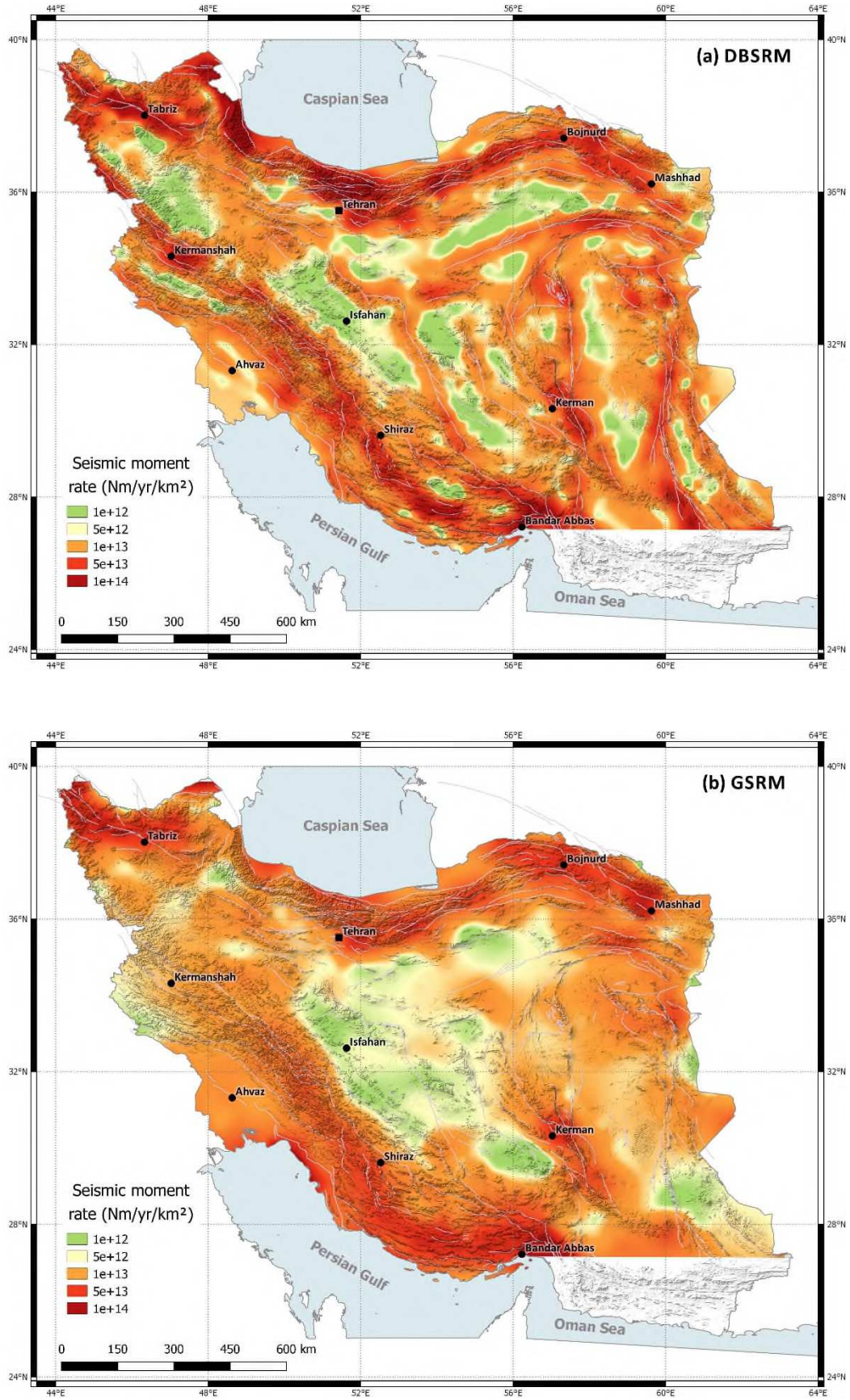

Figure 2. Moment rates ($\dot{M}_{0}^{\&D,total}$) for the Iranian Plateau based on: (a) DBSRM (Khodaverdian et al. 2015), (b) GSRM (Kreemer et al. 2014).

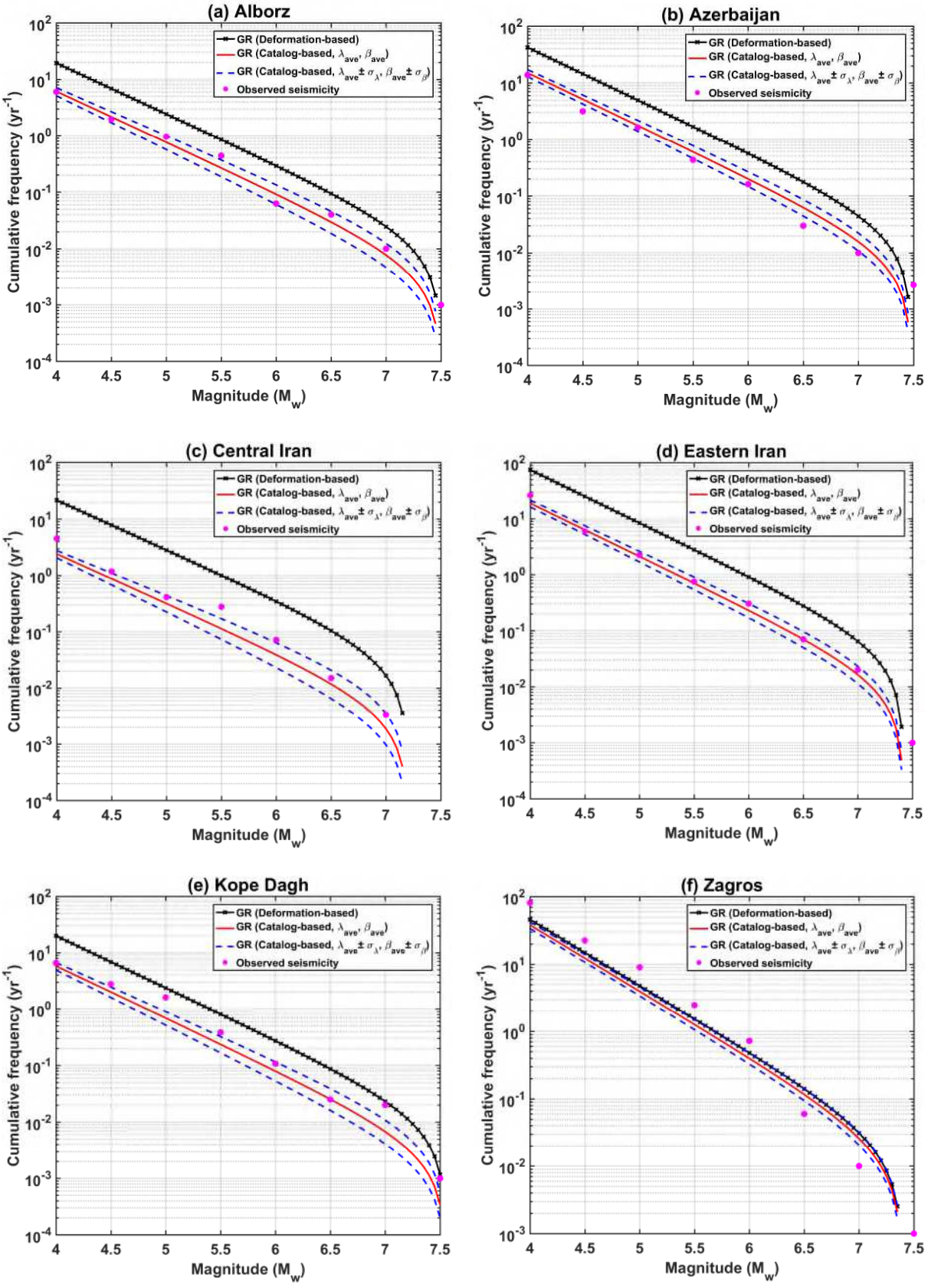

1123 **Figure 3. The frequency-magnitude distributions for different seismotectonic provinces.**

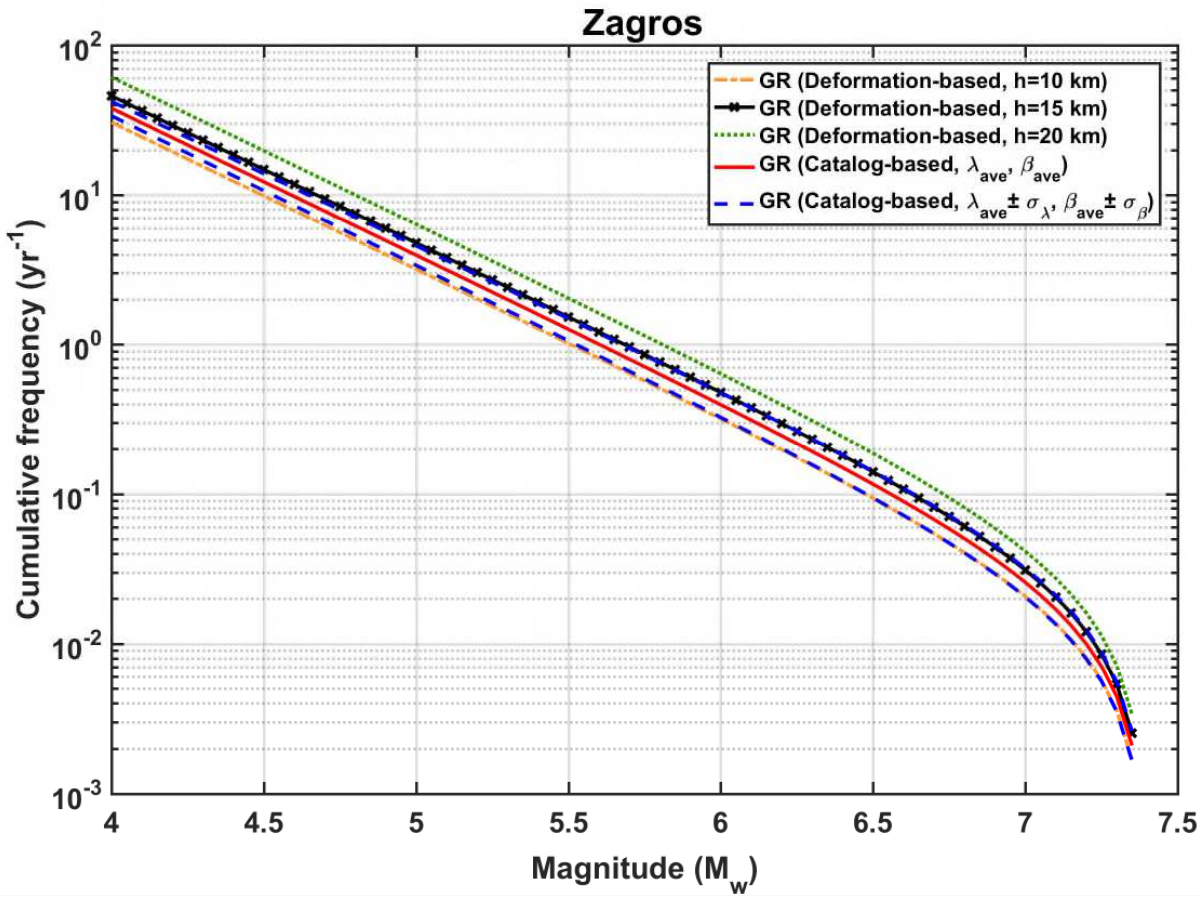

Figure 4. The frequency-magnitude distributions of earthquakes for the Zagros seismotectonic province.

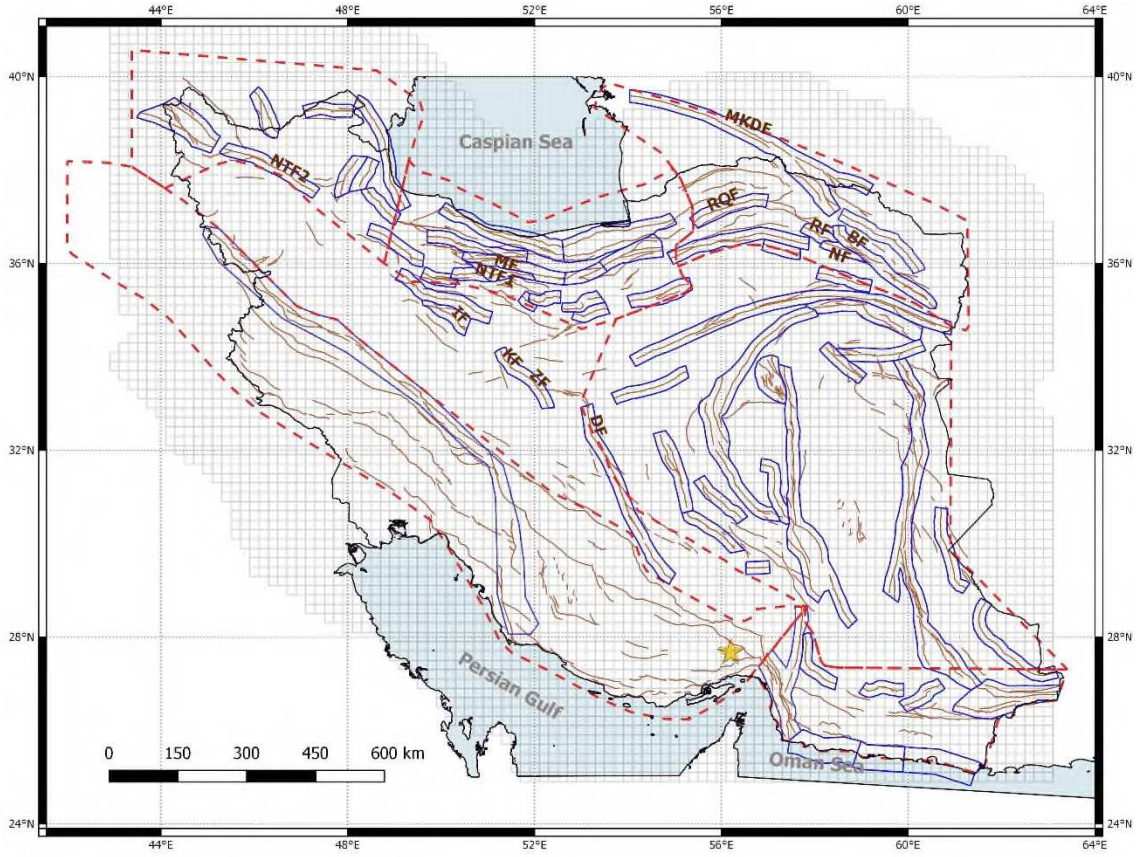

Figure 5. The area seismogenic sources are shown by gray squares. The light brown lines show the active faults. Near-fault zones are in solid blue lines. The red dashed lines show the seismotectonic provinces. The yellow star represents Finn, 2021 dual earthquakes. Main Kopeh Dagh Fault (MKDF), Robate-Qarabil Fault (RBF), Rivand Fault (RF), Neyshabur Fault (NF), Binalud Fault (BF), North Tehran Fault (NTF1), Mosha Fault (MF), North Tabriz Fault (NTF2), Dehshir Fault (DF), Kashan Fault (KF), Zefreh Fault (ZF), and Indes Fault (IF).

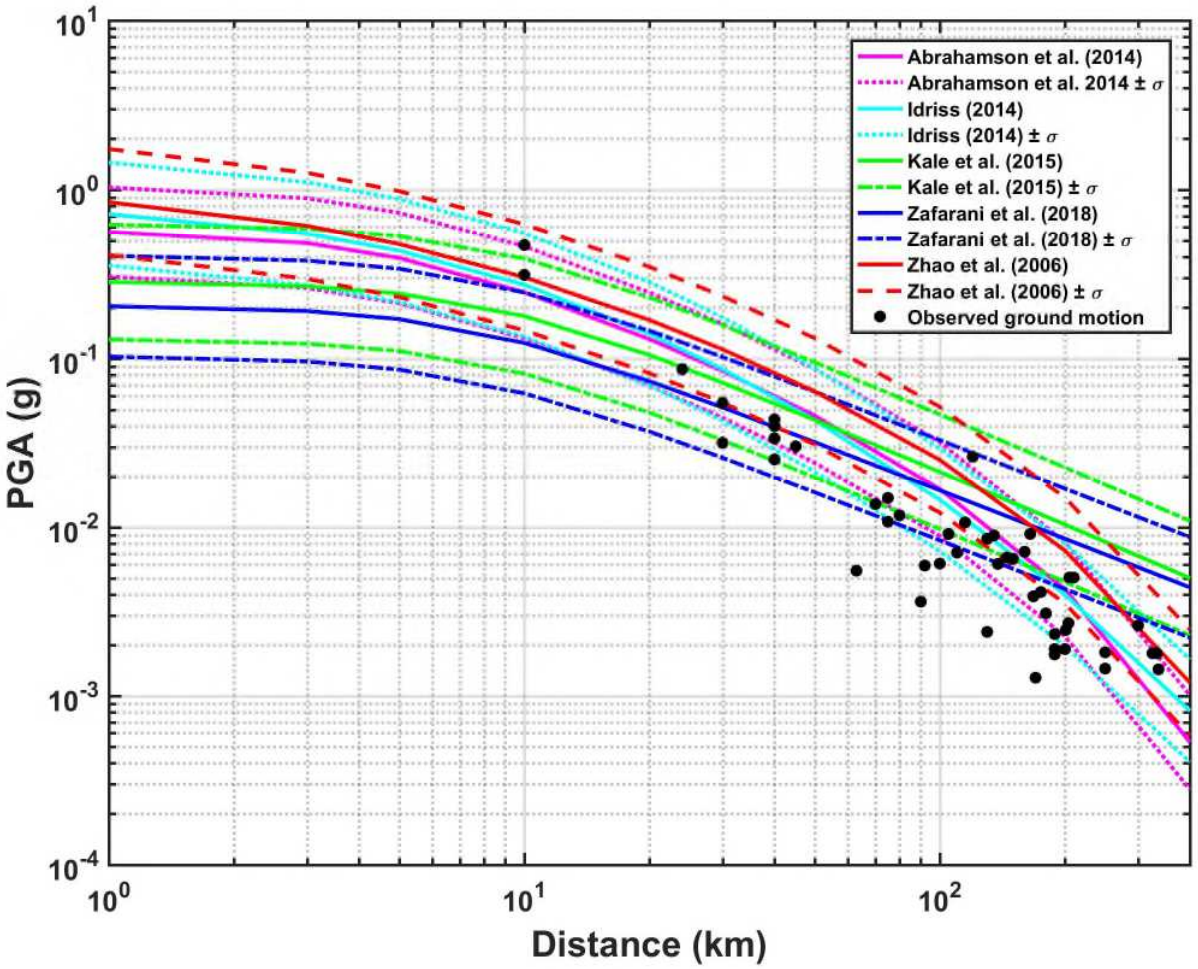

Figure 6. Ground motion recorded in the Finn, 2021 dual earthquakes and compaison to the five selected GMPEs: Abrahamson et al. (2014), Idriss (2014), Kale et al. (2015), Zafarani et al. (2018), and Zhao et al. (2006). The geometric mean of the east and north components are shown. Median and ± 1 sigma values from GMPEs are calculated for M6.2 with reverse focal mechanism and Vs30=500 m/s.

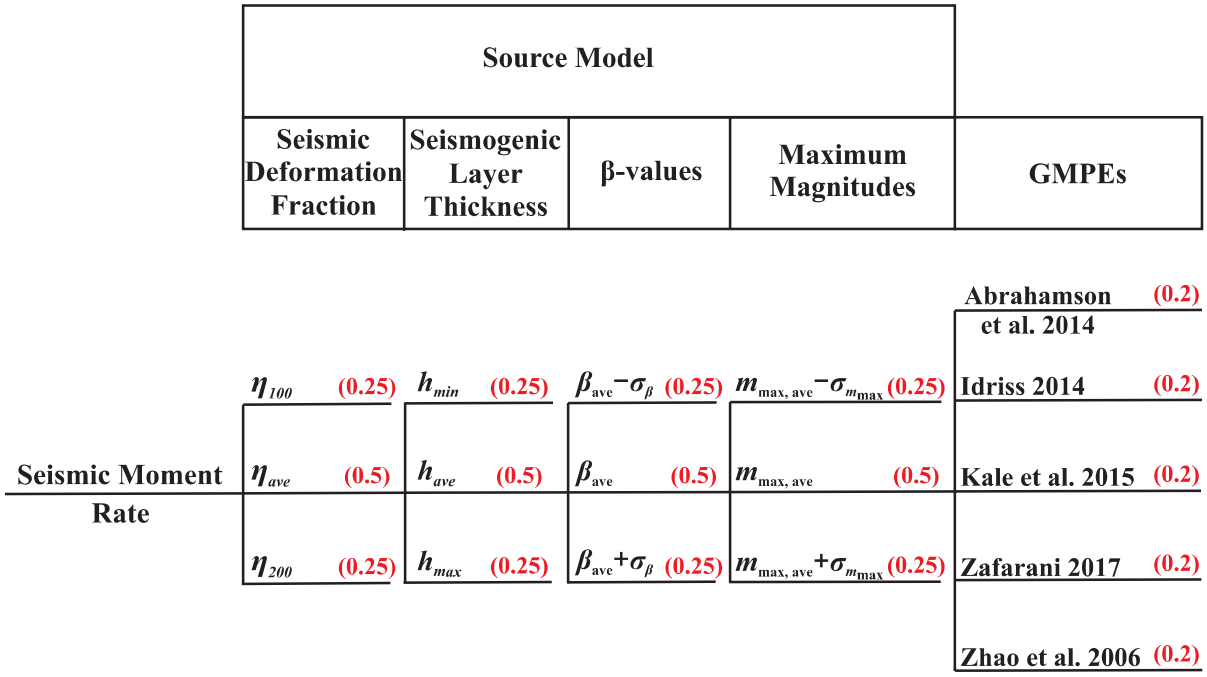

Figure 7. Hazard model logic tree. The red values show the weight of each branch.

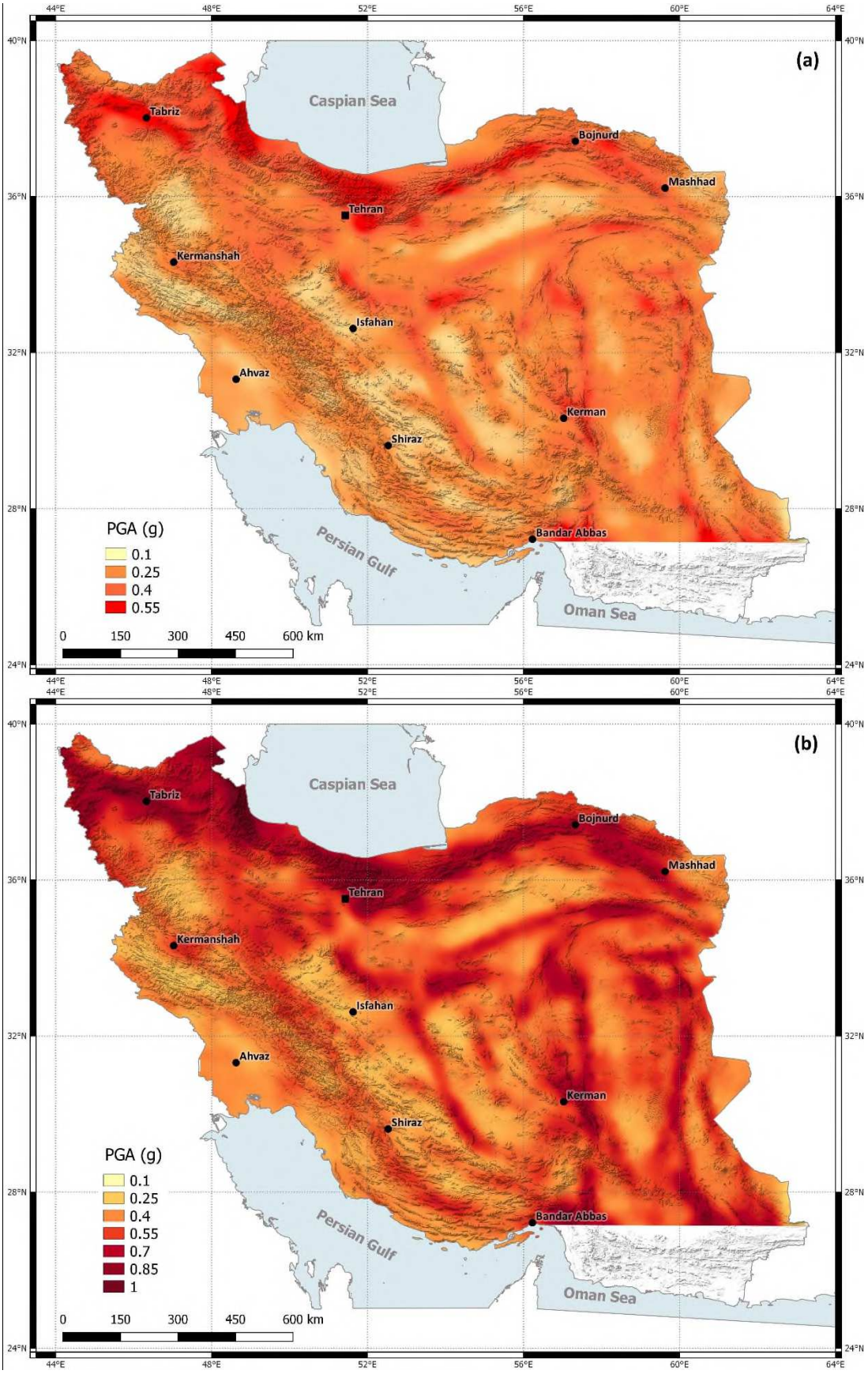

Figure 8. Mean PGA hazard map for the Iranian Plateau based on DBHM: (a) 10% POE in 50 years; (b) 2% POE in 50 years.

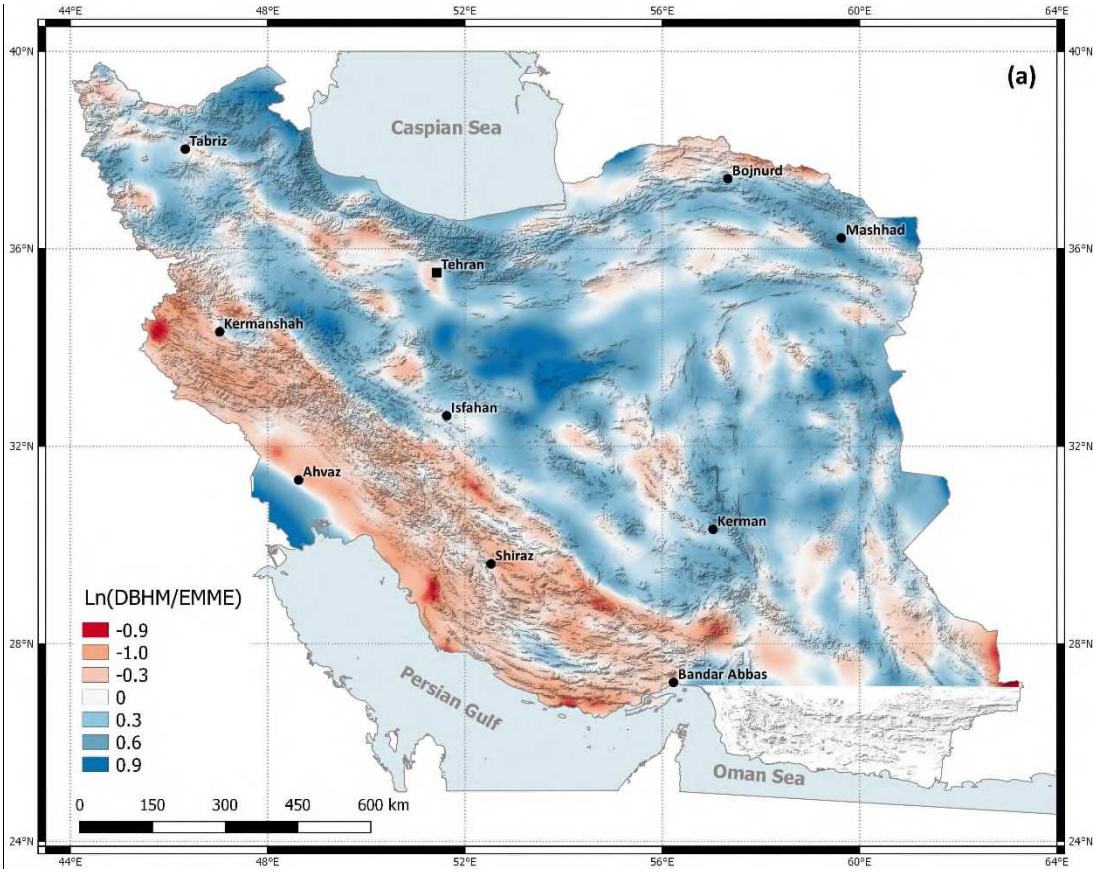

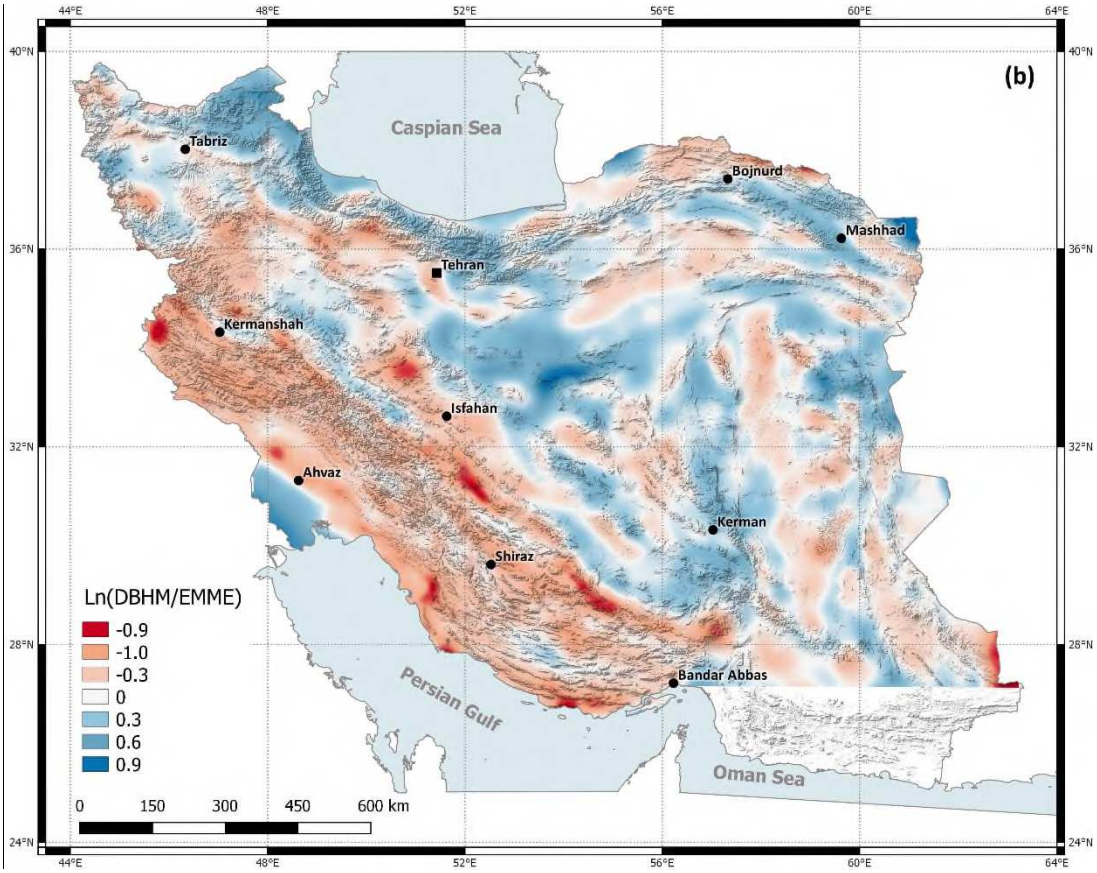

Figure 9. Ln(PGA_{DBHM}/PGA_{EMME}) for the Iranian Plateau: (a) 10% POE in 50 years; (b) 2% POE in 50 years.

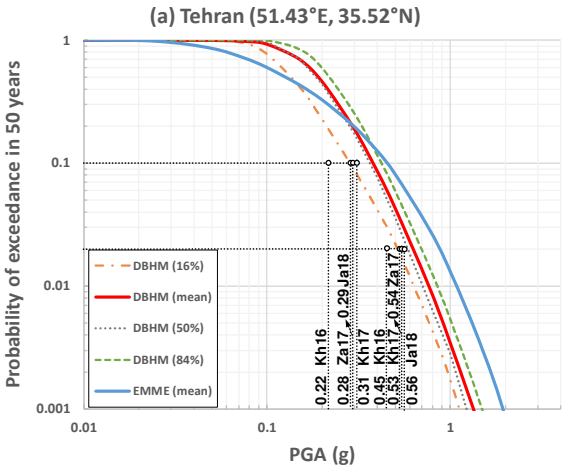
(a) Tehran (51.43°E, 35.52°N)
Probability of exceedance in 50 years
PGA (g)
DBHM (16%)
DBHM (mean)
DBHM (50%)
DBHM (84%)
EMME (mean)
0.22 Kh16
0.28 Za17
0.29 Ja18
0.31 Kh17
0.45 Kh16
0.53 Kh17
0.54 Za17
0.56 Ja18

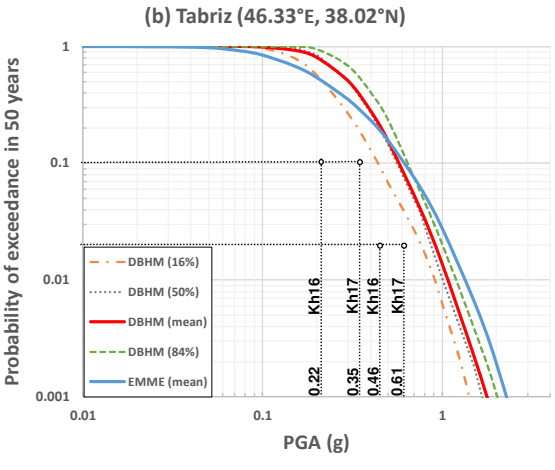
(b) Tabriz (46.33°E, 38.02°N)
Probability of exceedance in 50 years
PGA (g)
DBHM (16%)
DBHM (50%)
DBHM (mean)
DBHM (84%)
EMME (mean)
0.22 Kh16
0.35 Kh17
0.46 Kh16
0.61 Kh17

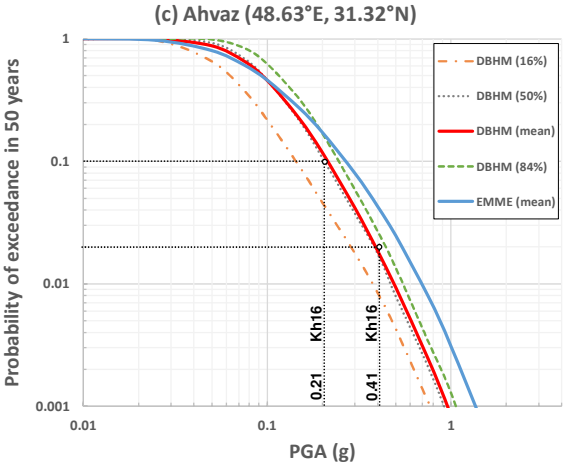
(c) Ahvaz (48.63°E, 31.32°N)
Probability of exceedance in 50 years
PGA (g)
DBHM (16%)
DBHM (50%)
DBHM (mean)
DBHM (84%)
EMME (mean)
0.21 Kh16
0.41 Kh16

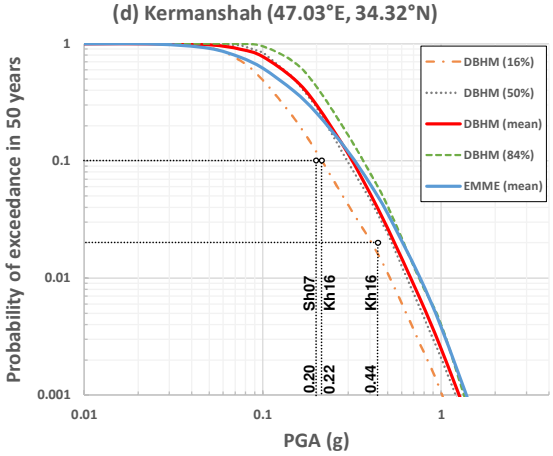
(d) Kermanshah (47.03°E, 34.32°N)
Probability of exceedance in 50 years
PGA (g)
DBHM (16%)
DBHM (50%)
DBHM (mean)
DBHM (84%)
EMME (mean)
0.20 Sh07
0.22 Kh16
0.44 Kh16

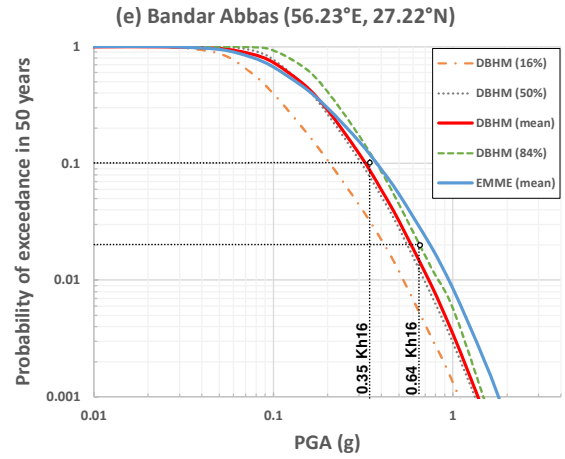
(e) Bandar Abbas (56.23°E, 27.22°N)
Probability of exceedance in 50 years
PGA (g)
DBHM (16%)
DBHM (50%)
DBHM (mean)
DBHM (84%)
EMME (mean)
0.35 Kh16
0.64 Kh16

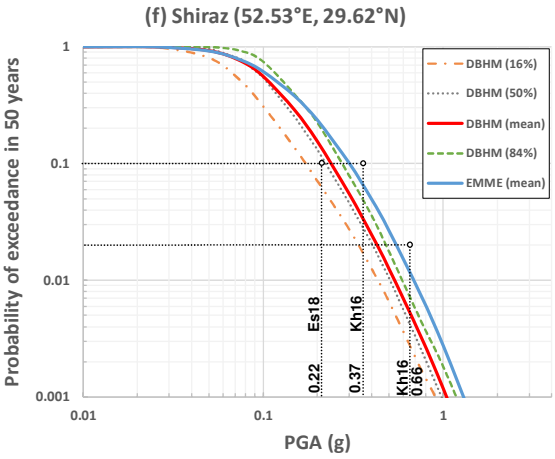
(f) Shiraz (52.53°E, 29.62°N)
Probability of exceedance in 50 years
PGA (g)
DBHM (16%)
DBHM (50%)
DBHM (mean)
DBHM (84%)
EMME (mean)
0.22 Es18
0.37 Kh16
0.66 Kh16

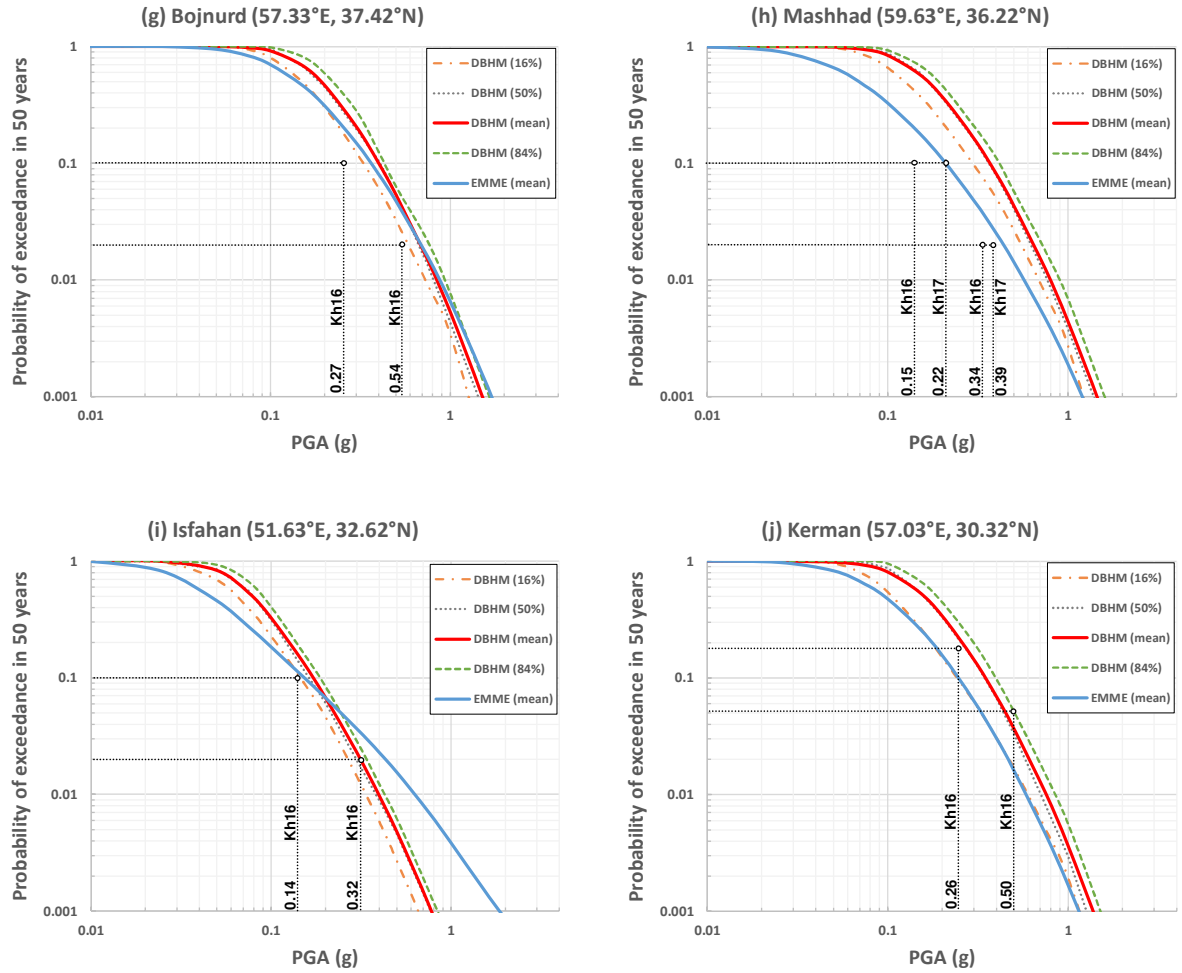

Figure 10. Hazard curves for important cities. DBHM: Deformation-Based Hazard Model, EMME: Earthquake Model of the Middle East, Sh07: (Shabani and Mirzaei 2007), Kh16: (Khodaverdian et al. 2016b), Kh17: (Khoshnevis et al. 2017), Za17: (Zafarani et al. 2017), Ja18: (Jalalalhosseini et al. 2018), and Es18: (Eskandarinejad et al. 2018).

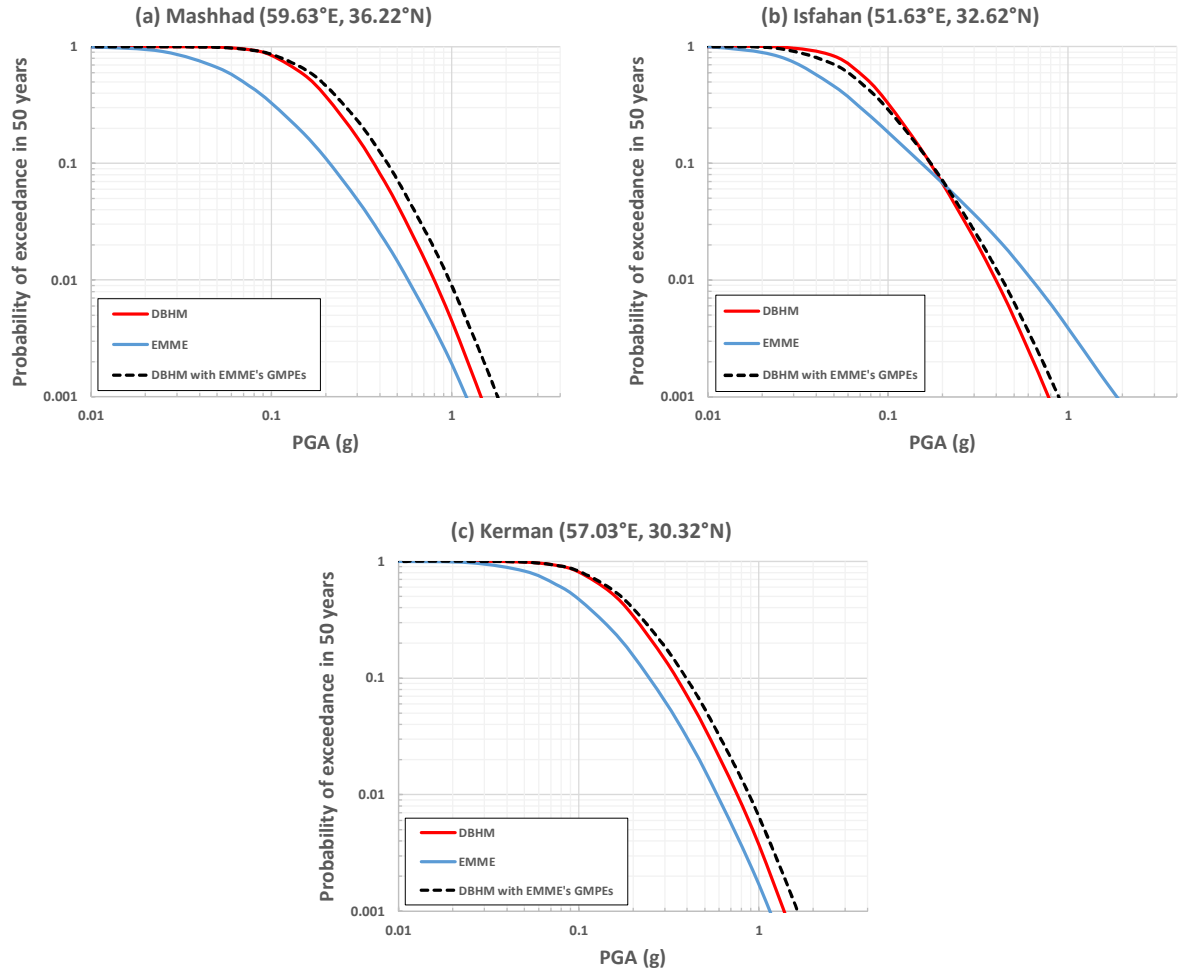

Figure 11. Mean hazard curves from DBHM, EMME, and modified DBHM with EMME's GMPEs.

Table 1. Seismic deformation fraction

Province	η_{100}	η_{200}	η_{ave}
Alborz	0.92	0.78	0.85
Azerbaijan	0.89	0.77	0.83
Central Iran	1.00	0.90	0.95
Eastern Iran	1.00	0.90	0.95
Kopeh Dagh	0.62	0.94	0.78
Zagros	0.39	0.28	0.34

η_{100} : seismic deformation fraction based on 100-years seismic catalog, η_{200} : seismic deformation fraction based on 200-years seismic catalog, η_{ave} : the average of η_{100} and η_{200} .

Table 2. Seismicity parameters and seismic moment rates, derived from the deformation-based model and observed seismicity

Province	β	$m_{\max}$	λ_4^C	$\dot{M}_0^C$ $(10^{17} Nm/yr)$	λ_4^D	$\dot{M}_0^D$ $(10^{17} Nm/yr)$	$\frac{\lambda_4^D}{\lambda_4^C}$	N_7^C	N_7^{D-C}
Alborz	2.08	7.5	6.10	12.59	19.36	40.30	3.17	0.77	1.67
Azerbaijan	2.14	7.48	14.95	26.16	42.02	74.30	2.81	1.56	2.83
Central Iran	2.02	7.20	2.41	3.71	21.39	33.25	8.88	0.19	1.47
Eastern Iran	2.18	7.42	18.80	27.79	74.22	111.15	3.95	1.63	4.80
Kopeh Dagh	2.13	7.55	5.81	11.42	19.91	39.50	3.43	0.67	1.63
Zagros	2.26	7.40	38.01	45.96	45.92	56.50	1.21	2.57	0.61

β : Slope of GR, $m_{\max}$: Maximum magnitude, λ_4^C : Catalog-based long-term earthquakes occurrence rates (for the magnitude equal to or larger than M_w 4.0), $\dot{M}_0^C$: Catalog-based long-term seismic moment rates, λ_4^D : Deformation-based earthquakes occurrence rates (for the magnitude equal to or larger than M_w 4.0), $\dot{M}_0^D$: Deformation-based seismic moment rates, N_7^C : Number of earthquakes with magnitude M_w 7.0 in 100 years derived from catalog-based occurrence rates, N_7^{D-C} : Number of earthquakes with magnitude M_w 7.0 in 100 years derived from difference between deformation-based and catalog-based occurrence rates.

Table 3. $\lambda^{D}_{m_0,h}$ for the seismogenic layer thickness of 10, 15, and 20 km

Province	$\lambda^{D}_{4,10}$	$\lambda^{D}_{4,15}$	$\lambda^{D}_{4,20}$
Alborz	12.91	19.36	25.81
Azerbaijan	28.01	42.02	56.03
Central Iran	14.26	21.39	28.52
Eastern Iran	49.48	74.22	98.96
Kopeh Dagh	13.27	19.91	26.55
Zagros	30.61	45.92	61.23

$\lambda^{D}_{m_0,h}$: Deformation-based earthquakes occurrence rates corresponding to the minimum magnitude m_0 and seismogenic layer thickness h.